Virologica Sinica 39 (2024) 56–70

Contents lists available at ScienceDirect

Virologica Sinica

journal homepage: www.keaipublishing.com/en/journals/virologica-sinica
www.virosin.org

Research Article

Mutual antagonism of mouse-adaptation mutations in HA and PA proteins on H9N2 virus replication

Liping Ma [a,b,d], Huabin Zheng [a,b,d], Xianliang Ke [a,b], Rui Gui [a,b,d], Zhongzi Yao [a,b,d], Jiasong Xiong [a,b,d], Quanjiao Chen [a,b,c,*]

[a] CAS Key Laboratory of Special Pathogens and Biosafety, Wuhan Institute of Virology, Chinese Academy of Sciences, Wuhan, 430207, China
[b] Center for Biosafety Mega-Science, Wuhan Institute of Virology, Chinese Academy of Sciences, Wuhan, 430207, China
[c] Hubei Jiangxia Laboratory, Wuhan, 430207, China
[d] University of Chinese Academy of Sciences, Beijing, 100049, China

ARTICLE INFO

Keywords:
Influenza A virus (IAV)
H9N2
HA
PA
Antagonism
Mouse adaptation

ABSTRACT

Avian H9N2 viruses have wide host range among the influenza A viruses. However, knowledge of H9N2 mammalian adaptation is limited. To explore the molecular basis of the adaptation to mammals, we performed serial lung passaging of the H9N2 strain A/chicken/Hunan/8.27 YYGK3W3-OC/2018 (3W3) in mice and identified six mutations in the hemagglutinin (HA) and polymerase acidic (PA) proteins. Mutations L226Q, T511I, and A528V of HA were responsible for enhanced pathogenicity and viral replication in mice; notably, HA-L226Q was the key determinant. Mutations T97I, I545V, and S594G of PA contributed to enhanced polymerase activity in mammalian cells and increased viral replication levels *in vitro* and *in vivo*. PA-T97I increased viral polymerase activity by accelerating the viral polymerase complex assembly. Our findings revealed that the viral replication was affected by the presence of PA-97I and/or PA-545V in combination with a triple-point HA mutation. Furthermore, the double- and triple-point PA mutations demonstrated antagonistic effect on viral replication when combined with HA-226Q. Notably, any combination of PA mutations, along with double-point HA mutations, resulted in antagonistic effect on viral replication. We also observed antagonism in viral replication between PA-545V and PA-97I, as well as between HA-528V and PA-545V. Our findings demonstrated that several antagonistic mutations in HA and PA proteins affect viral replication, which may contribute to the H9N2 virus adaptation to mice and mammalian cells. These findings can potentially contribute to the monitoring of H9N2 field strains for assessing their potential risk in mammals.

1. Introduction

The H9N2 virus is a low pathogenic avian influenza virus (AIV). H9N2 was first isolated in 1966 and has since spread across terrestrial poultry populations in Eurasia and Africa, causing sporadic infections in humans and mammals (Homme and Easterday, 1970; Liu et al., 2003; Xu et al., 2007). After its first isolation in China in 1994, over 20 years of dissemination and evolution have seen H9N2 replace the H7N9 and H5N6 viruses as the predominant subtype among Chinese poultry during 2016–2019 (Bi et al., 2020; Hu et al., 2021). H9N2 can infect humans directly and cause respiratory diseases with varying degrees of severity. The first human case of H9N2 infection was reported in China in 1998, with several subsequent cases reported in China (Peiris et al., 1999; Butt et al., 2005; Huang et al., 2015; Yuan et al., 2017; Pan et al., 2018; Guo et al., 2020), Pakistan (Ali et al., 2019), India (Potdar et al., 2019), Oman (Almayahi et al., 2020), Bangladesh (Shanmuganatham et al., 2013), Cambodia (Um et al., 2021), Egypt (Gomaa et al., 2020), and Senegal (Jallow et al., 2020) in the following 20 years. Previous studies have revealed that H9N2 viruses can contribute internal genes to other subtypes of AIV. For instance, the novel reassortant H7N9 virus, which emerged in 2013, contains all six internal genes derived from the H9N2 virus (Lam et al., 2013; Liu et al., 2013) and has caused over 1500 human infections with a fatality rate of approximately 40% as of January 13, 2023 (Chang et al., 2023). The H10N8 virus, which has caused human infection and death, also has six internal genes derived from H9N2 (Chen et al., 2014). Other AIV subtypes that have received internal genes from H9N2 include the 1997 Hong Kong H5N1 (Guan et al., 1999), 2015 Guangdong H5N6 (Shen et al., 2016) and recent H3N8 (Yang et al., 2022).

* Corresponding author.
E-mail address: chenqj@wh.iov.cn (Q. Chen).

https://doi.org/10.1016/j.virs.2023.11.004
Received 14 July 2023; Accepted 10 November 2023
Available online 13 November 2023

Serological investigations have indicated that more humans have been infected with the H9 subtype than with the H5 and H7 subtypes (Li et al., 2017; Ma et al., 2018; Song and Qin, 2020). H9 seropositivity is particularly common among poultry market workers in southern China (Li et al., 2017; Ma et al., 2018; Song and Qin, 2020), suggesting that direct exposure is a risk factor for H9N2 infection. In poultry, the hemagglutinin (HA) receptor preference of most H9N2 viruses seemed to have gained the ability to bind human-receptor (Gao et al., 2021), indicating an increased risk of cross-species transmission to mammals. Though some studies have described the molecular mechanisms associated with the adaptation of H9N2 viruses to mammals, the molecular basis remains to be supplemented.

The mechanism of viral adaptation to mammals can be effectively explored by serially passaging AIVs in the lungs of mice (Brown et al., 2001). In this study, we explored the molecular basis of H9N2 mammalian adaptation by passaging an A/chicken/Hunan/8.27 YYGK3W3-OC/2018 (3W3) virus (isolated from chickens during routine monitoring at a live poultry market) in mouse lungs and analyzing the dynamic changes in virus performance. Six mutations were identified in HA and polymerase acidic (PA) proteins, and were responsible for the enhanced pathogenicity and replication capacity of the 3W3 mouse-adapted virus. Furthermore, we found that antagonism between some mutations in HA and PA proteins to viral replication during the adaptation process. We believe our findings may have implications for field monitoring H9N2 viruses with respect to assessing their potential risk.

2. Materials and methods

2.1. Cells and viruses

Madin–Darby canine kidney (MDCK) cells, adenocarcinomic human alveolar basal epithelial (A549) cells and human embryonic kidney (293T) cells were originally sourced by our laboratory, and chicken immortal fibroblasts (DF-1) cells were generously provided by professor Meilin Jin (Huazhong Agricultural University). All cells were maintained in Dulbecco's modified Eagle's medium (DMEM) with 10% fetal calf serum and incubated at 37 °C in 5% CO_2.

A/chicken/Hunan/8.27 YYGK3W3-OC/2018 (H9N2) (3W3), was isolated from a live poultry market (Bi et al., 2020). Virus stocks were propagated in 10-d-old specific-pathogen-free (SPF) embryonated chicken eggs (Boehringer Ingelheim, Beijing, China) at 38 °C for 72 h. The allantoic fluid was harvested and purified using the limiting dilution method to obtain the monoclonal 3W3 virus (or P0 virus), which was aliquoted and stored at −80 °C. Virus titers were measured using a plaque assay in MDCK cells. All experiments involving live viruses were performed in BSL-2 facilities at the Wuhan Institute of Virology, Chinese Academy of Sciences, Wuhan, China.

2.2. Antibodies

The antibodies used in this study were as follows: DDDDK Tag mouse antibody (66008-3-Ig, Proteintech, Wuhan, China), GAPDH mouse antibody (60004-1-Ig; Proteintech, Wuhan, China), Monoclonal Anti-HA antibody produced in mice (H3663-100UL, Sigma-Aldrich), and Influenza A virus PB1 protein antibody (GTX125923, Genetex, Alton Pkwy Irvine, CA, USA) with a dilution at 1:1000.

2.3. Mouse adaptation of the 3W3 virus

Five 6-week-old female SPF BALB/c mice (Slac laboratory animal, Shanghai, China) were anesthetized via intraperitoneal injection with 2.5% avertin and inoculated intranasally with 50 μL of 10-fold-diluted P0 virus in phosphate buffer saline (PBS) supplemented with 0.1% bovine serum albumin (BSA). Mice were euthanized at day 3 post inoculation (d.p.i.), and their lungs were collected. Each lung was washed 10 times with 2 mL 0.1% BSA-PBS to obtain the bronchoalveolar lavage fluid (BALF). The BALF was centrifuged (10,000 ×*g* for 10 min at 4 °C), and the supernatant was collected to isolate the P1 virus. Five mice were simultaneously prepared for the next passage and inoculated intranasally with 50 μL of the P1 virus. After five passages, the mice died within 4 days, and all the obtained viruses (P0–P5) were utilized for subsequent experiments.

2.4. Viral genome sequencing

The RNA of P0–P5 viruses was extracted using the MiniBEST Viral RNA/DNA Extraction Kit v5.0 (9766, Takara Bio, Tokyo, Japan). One-step reverse transcription-polymerase chain reaction (RT-PCR) was performed as described before (Bi et al., 2016) using conserved primers (Kampmann et al., 2011) that could amplify all eight genes of the influenza A virus. RT-PCR products were verified by agarose gel electrophoresis and then stored on dry ice for next-generation sequencing (NGS).

2.5. Reverse genetics

Based on the sequence analysis, P0, P3, and P5 viruses were generated by plasmid-based reverse genetics, as previously described (Hoffmann et al., 2000). Eight genes of P0, P3, and P5 viruses were amplified using segment-specific primers and cloned into the pHW2000 vector by homologous recombination using a Clone Express II one-step cloning kit (C112-02, Vazyme, Nanjing, China). Mutations in *HA* and *PA* genes were introduced by PCR-based directed mutagenesis with point mutation primer sets (Supplementary Table S1) and verified by Sanger sequencing.

293T and MDCK cells plated 2:1 in 6-well plates at approximately 90% confluence were transfected with a mixture of pHW2000-PB2, PB1, PA, HA, NP, NA, M, and NS plasmids of each virus (0.5 μg of each plasmid) using Lipo8000 Transfection Reagent (C0533, Beyotime, Haimen, China) following the manufacturer's instructions. After 24 h, the supernatant of the transfected cells was replaced with virus maintenance solution in the presence of 0.5 μg/mL tosylsulfonyl phenylalanyl chloromethyl ketone (TPCK)-trypsin (LS003740, Worthington, Lakewood, NJ, USA). At 72 h.p.i., supernatants containing rescued viruses were harvested and propagated in MDCK cells plated in a 25 cm^2 tissue flask in the presence of 2 μg/mL TPCK-trypsin at 37 °C for 72 h. Subsequently, the recombinant virus-containing supernatants were aliquoted and confirmed by sequencing. Viral titers were measured using a plaque assay in MDCK cells, and no difference in the plaque morphology of all recombinant viruses was observed.

2.6. Plaque assay

MDCK monolayers were plated in 24-well plates at 2.5 × 10^5 cells/well, resulting in a cell density of approximately 95%–100% after 12 h. The cells were washed twice with PBS, and infected with 100 μL of diluted viruses at 37 °C for 1 h, and shook diagonally every 15 min. After 1 h, remove the virus inoculum and wash the cell twice with PBS. Then, the cells were overlaid with 1 × plaque maintenance solution containing MEM with 0.3% BSA, 1% low melting point agarose and 2 μg/mL TPCK-treated Trypsin. After the maintenance solution complete coagulation at 18–26 °C, invert the plates at 37 °C incubator for 48 h, and then count the number of plaques. Five to fifty plaques per well are considered relatively accurate.

2.7. Mouse pathogenicity experiments

Each virus was diluted to 1 × 10^5 PFU/50 μL in 0.1% BSA-PBS. Eight 4–6-week-old female SPF BALB/C mice were divided into different treatment groups (five for weight monitoring and three for dissection). All mice were weighed before the challenge and anesthetized by intraperitoneal injection of 2.5% avertin at 150 μL/10 g. After anesthesia,

each mouse was intranasally infected with 50 μL of diluted virus solution. The mice were dissected at 3 d.p.i., and their heart, liver, spleen, lung, kidney, nasal turbinate, brain, and intestine were harvested for homogenization. The supernatant of the homogenates was used for the plaque assay on MDCK cells to determine the virus titer in each tissue. A small amount of lung tissue was collected for histopathological analysis. Mice in the weight-monitoring group were weighed at the same time point every day after infection for 14 days. During this period, mice losing ≥25% of their body weight were sacrificed.

2.8. Viral growth kinetics

A549 or DF-1 cells were plated in 24-well plates at 2×10^5 cells/well, resulting in a cell density of approximately 85%–95% after 12 h. The viruses were diluted with DMEM containing 0.3% BSA and 2 μg/mL TPCK-trypsin to 0.01 MOI (multiplicity of infection) and inoculated into the monolayers at 37 °C for 1 h. The back titration was performed using absolute quantitative qPCR to detect the copy number of NP vRNA of recombinant viruses to confirm the comparable plaque to genome ratios. The pHW2000-NP was used as standard, and the primers for NP vRNA detection are shown in Supplementary Table S1. The virus solution was discarded after 1 h incubation, the cells were washed twice, and 500 μL of virus maintenance solution (with a final concentration of TPCK-treated trypsin of 0.5 μg/mL) was added to each well, and then incubated at 37 °C with 5% CO_2. Supernatants were collected at 12 h, 24 h, 48, and 72 h.p.i. and stored at −80 °C, and the titers were determined by plaque assay on MDCK cells. In order to confirm the comparability, the viral growth kinetics of the recombinant viruses was tested with rP0 virus together in each separate experiment.

2.9. RNP activity assay

293T and DF-1 cells were plated in a 12-well plate at 5×10^5 cells/well, resulting in a cell density of approximately 85%–95% after 12 h. The 293T or DF-1 cell monolayers were transfected with 0.3 μg pCDNA3.1-PB2, 0.3 μg pCDNA3.1-PB1, or 0.4 μg pCDNA3.1-PA of various combinations of *PA* mutations and 0.2 μg pCDNA3.1-NP, and 0.3 μg fluorescent reporter plasmids (provided by Professor Meilin Jin from Huazhong Agricultural University, Wuhan, China) pPoll-NS-Luc (for 293T cells) or pPol I-AVI (for DF-1 cells) and 5 ng pRL-TK using Lipo8000 transfection reagent according to the manufacturer's instructions. After 24 h of transfection, the cells were washed once with 4 °C pre-cooled PBS and fully lysed with 200 μL diluted 1 × passive lysis buffer by shaking on ice for 15 min. Dual fluorescence was measured using a Promega GLOMAX 20/20 Luminometer with the Dual Luciferase Reporter Assay System (E1960, Promega, Beijing, China).

2.10. Receptor-binding assay

Receptor-binding specificity of recombinant viruses was examined using the solid-phase direct binding assay as described previously (Bi et al., 2015; Yao et al., 2022). Briefly, 96-well microtiter plates were coated with biotinylated glycan α-2,3-SA receptor (trisaccharide, Neu5Acα2-3Galβ1-4GlcNAcβ-SpNH-LC-LC-biotin, and pentasaccharide, NeuAcα2-3Galβ1-4GlcNAcβ1-3Galβ1-4GlcNAcβ1-SpNH-LC-LC-biotin) (0036-BP, GlycoNZ, Auckland, New Zealand) and α-2,6-SA receptor (trisaccharide, Neu5Acα2-6Galβ1-4GlcNAcβ-SpNH-LC-LC-biotin, and pentasaccharide, NeuAcα2-6Galβ1-4GlcNAcβ1-3Galβ1-4GlcNAcβ1-SpNH-LC-LC-biotin) (0997-BP, GlycoNZ, Auckland, New Zealand). Virus diluents containing 64 hemagglutinin units were incubated with neuraminidase inhibitors (oseltamivir and zanamivir) at final concentrations of 100 nmol/L. Virus-receptor binding was determined using mouse antisera against 3W3 recombinant viruses and horseradish peroxidase (HRP)-linked goat anti-mouse IgG (H+L) (AS003, Abclonal, Wuhan, China). Tetramethylbenzidine (TMB) was used as the substrate, and the absorbances were measured at 450 nm.

2.11. Co-immunoprecipitation

293T cells were plated onto a six-well plate at 1×10^6 cells/well, resulting in a cell density of approximately 85%–95% after 12 h; 293T cell monolayers were transfected with plasmids using Lipo8000. At 24 h.p.i., cells were washed with 4 °C pre-cooled PBS and fully lysed with 300 μL IP lysis buffer containing protease inhibitor cocktail (HY-K0010-hd, MedChemExpress, Princeton, NJ, USA) on ice for 15 min. The lysate supernatant was incubated with anti-HA magnetic beads (HY-K0201, MedChemExpress, Princeton, NJ, USA) for 4 h at 4 °C. The beads were collected and washed four times with 4 °C-pre-cooled PBST buffer and then boiled with 50 μL 1× SDS loading buffer for 10 min. Finally, protein levels were determined by Western blotting.

2.12. Statistical analysis

Three individual replicates were performed in *in vitro* assay. A two-tailed unpaired *t*-test or one-way analysis of variance (ANOVA) was used to assess differences between groups in GraphPad Prism v8.3.0, with statistical significance set at *P*-value <0.05.

3. Results

3.1. Adaptation of 3W3 H9N2 virus in mice and mutation analysis of mouse-adapted 3W3 viruses

To determine the mechanisms of H9N2 virus adaptation to mammals, we passaged the 3W3 virus (isolated from chickens during routine monitoring at a live poultry market; wild type [WT]: P0 virus) in BALB/c mice for five generations (P1, P2, P3, P4, and P5). Mice infected with the WT 3W3 virus (P1 group) exhibited no clinical signs or weight loss, similar to the mock-infected group (Fig. 1). In contrast, the P2, P3, P4, and P5 groups displayed classic clinical signs of infection, including huddling, hunched posture, less movement, and ruffled fur, and showed significant weight loss (Fig. 1A). In the P2 and P4 groups, mice died from 5 d.p.i. and all mice died within 7 d.p.i. (Fig. 1B). All mice infected with P3 died at 4 d.p.i., mice in the P5 group died from 1 d.p.i., and all died within 4 d.p.i. (Fig. 1A and B).

The whole genomes of P0 and mouse-adapted viruses (P1, P2, P3, P4, and P5) were sequenced and aligned. Sequence alignment revealed that P0 and P1, P2 and P3 viruses, and P4 and P5 possessed the same genome, respectively. Three HA mutations (L226Q, T511I, and A528V, H3 numbering; L216Q, T503I, and A520V, H9 numbering, cut signal peptide) were observed in the P2 and P3 viruses. Six amino acid substitutions, three in HA (L226Q, T511I, and A528V, H3 numbering) and three in PA (T97I, I545V, and S594G), were identified in the P4 and P5 viruses (Fig. 1C).

The HA-226 residue was located in the receptor-binding sites of the HA1 domain, and the HA-511 and HA-528 residues were both located in the HA2 domain (Fig. 1D). For PA, 97 residues were located in the PB2 binding motif (1–100 residues) (Hemerka et al., 2009) and also in endonuclease domain (1–197 residues) (Dias et al., 2009) of the N-terminal subunit (1–256 residues) (Fig. 1D), and 545 and 594 residues were located in the C-terminal subunit of PA (277–716 residues) (Fig. 1D).

We assessed these mutations in clinically isolated H9N2 strains containing all mammalian (including human) and avian H9N2 strains isolated worldwide with complete amino acid sequences of both HA and PA proteins as of September 7, 2023 (GISAID database, https://gisaid.org). Mutation analysis covered 26 HA and 26 PA amino acid sequences of mammalian H9N2 viruses, as well as 849 HA and 849 PA amino acid sequences of avian H9N2 isolates (all strains are described in Supplementary Dataset S1).

HA-226Q was found in 50.00% of mammalian H9N2 and 20.73% of avian H9N2 isolates, respectively (Supplementary Fig. S1A, Dataset S1). Both HA-511I and PA-594G were not observed in mammalian H9N2 isolates but occurred in 1.53% and 0.12% of the avian H9N2 viruses,

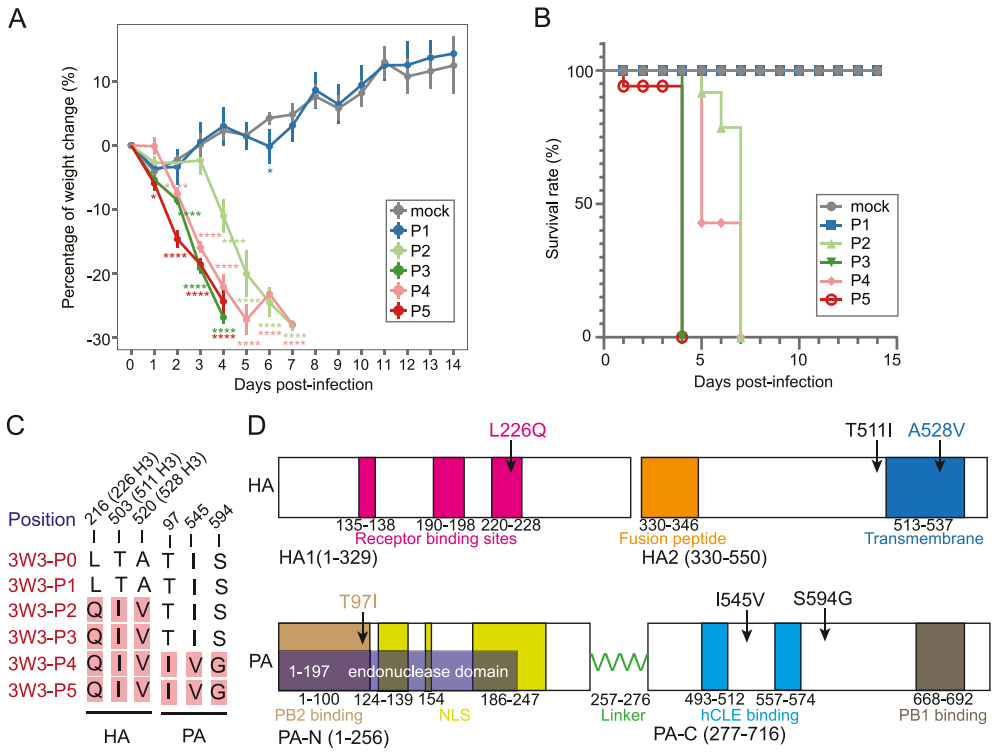

Fig. 1. Generation and sequence analysis of mouse-adapted 3W3 virus. Five-week-old female BALB/c mice (n = 5 per group) was inoculated intranasally with 50 μL 3W3 P0 virus and isolated the P1 virus from lung lavage fluid at 3 d.p.i. Then the virus was passaged another four generations to obtain viruses P2 to P5, with lung lavage fluid collected at 3 d.p.i. of each passage. The mock group (n = 5) was inoculated intranasally with 50 μL 0.1% BSA-PBS. Body weight loss (**A**) and survival rates (**B**) were observed over 14 days. Mice lost ≥25% of their body weight were considered as dead and sacrificed. Significant body weight changes between virus-infected and mock group mice (Student's *t*-test, two-tailed) are indicated by $*P < 0.05$, $**P < 0.01$, $***P < 0.001$, and $****P < 0.0001$. **C** Mutations detected in 3W3-mouse adapted viruses indicated on the pink background, and the positions of HA proteins are labeled with both H9 and H3 numbering (cut signal peptide). **D** Primary structural locations of the amino acid substitutions identified in the 3W3 mouse-adapted virus and the functional domains of HA (H3 numbering) and PA proteins are indicated. NLS, nuclear localization signal; hCLE, human transcription factor (interacts with PA at two indicated regions (Huarte et al., 2001; Ping et al., 2011)).

respectively (Supplementary Fig. S1A and S1B, Dataset S1). However, neither HA-528V nor PA-97I was found in both mammalian and avian H9N2 isolates (Supplementary Fig. S1A and S1B, Dataset S1). The prevalence of PA-545V in mammalian H9N2 viruses (26.92%) was significantly greater than that of avian H9N2 isolates (8.24%) (Supplementary Fig. S1B, Dataset S1).

3.2. Replication and pathogenicity of rescued P3 and P5 recombinant viruses in vitro and in vivo

To verify the function of the mutation sites in HA and PA, we rescued the 3W3 WT virus (rP0) and mouse-adapted P3 and P5 viruses (rP3 and rP5). The growth kinetics of rP3 and rP5 viruses in A549 and DF-1 cells indicated that they replicated to significantly higher titers than those of the rP0 virus (Fig. 2A), suggesting that 3W3 mouse-adapted viruses acquired increased replication capacity in both mammalian and avian cells. Notably, the replication capacity of the rP3 virus was slightly higher than that of the rP5 virus *in vitro* (Fig. 2A).

We tested the pathogenicity of the rescued viruses *in vivo*. The viral titers in the lungs and nasal turbinates of rP3 and rP5 mice were similar and were significantly higher than those of rP0-infected mice (Fig. 2B). All mice infected with rP0 survived, and no body weight loss was observed. However, mice inoculated with rP3 and rP5 viruses showed severe clinical signs and significant weight loss, and all died within 6 and 4 d.p.i., respectively (Fig. 2C and D).

Histopathological examination of the lungs of infected mice at 3 d.p.i. indicated that the rP0 virus did not cause lung injury (Fig. 2E). In contrast, the lungs of mice inoculated with the rP3 virus revealed an alveolar blockage, thickening of alveolar walls, hemorrhage, and inflammatory cell infiltration (Fig. 2E). A more severe degree of lung tissue injury, including the thickening of alveolar walls, infiltration of inflammatory cells, and hemorrhage (Fig. 2E), was observed in rP5-infected mice. These results suggest that the 3W3 mouse-adapted virus has a higher replication capacity *in vitro* and increased virulence *in vivo*.

3.3. HA-L226Q, T511I, and A528V were responsible for enhanced pathogenicity in mice

To identify the mutations responsible for the enhanced replication capacity and pathogenicity of the H9N2 mouse-adapted virus, we generated two recombinant viruses containing P3HA or P5PA segments in a P0 background, namely rP0-P3HA (whole genome identical to that of the P3 and rP3 virus) and rP0-P5PA, respectively (Fig. 3A). The growth curves in A549 and DF-1 cells indicated that the titers of rP0-P3HA and rP0-P5PA were significantly higher than those of the rP0 virus (Fig. 3B and C). The rP0-P5PA virus exhibited stronger replication capability in A549 cells compared with that of the rP0-P3HA virus; however, in DF-1 cells, the replication capability of the rP0-P5PA virus was weaker than that of the rP0-P3HA virus (Fig. 3B and C).

The titers in the lungs and nasal turbinates of mice infected with the rP0-P3HA and rP0-P5PA viruses were significantly higher than those of mice infected with the rP0 virus (Fig. 3D). rP0-P3HA-inoculated mice showed typical clinical features of infection and significant weight loss, and all died within 6 d.p.i. (Fig. 3E and F). Consistent with that in

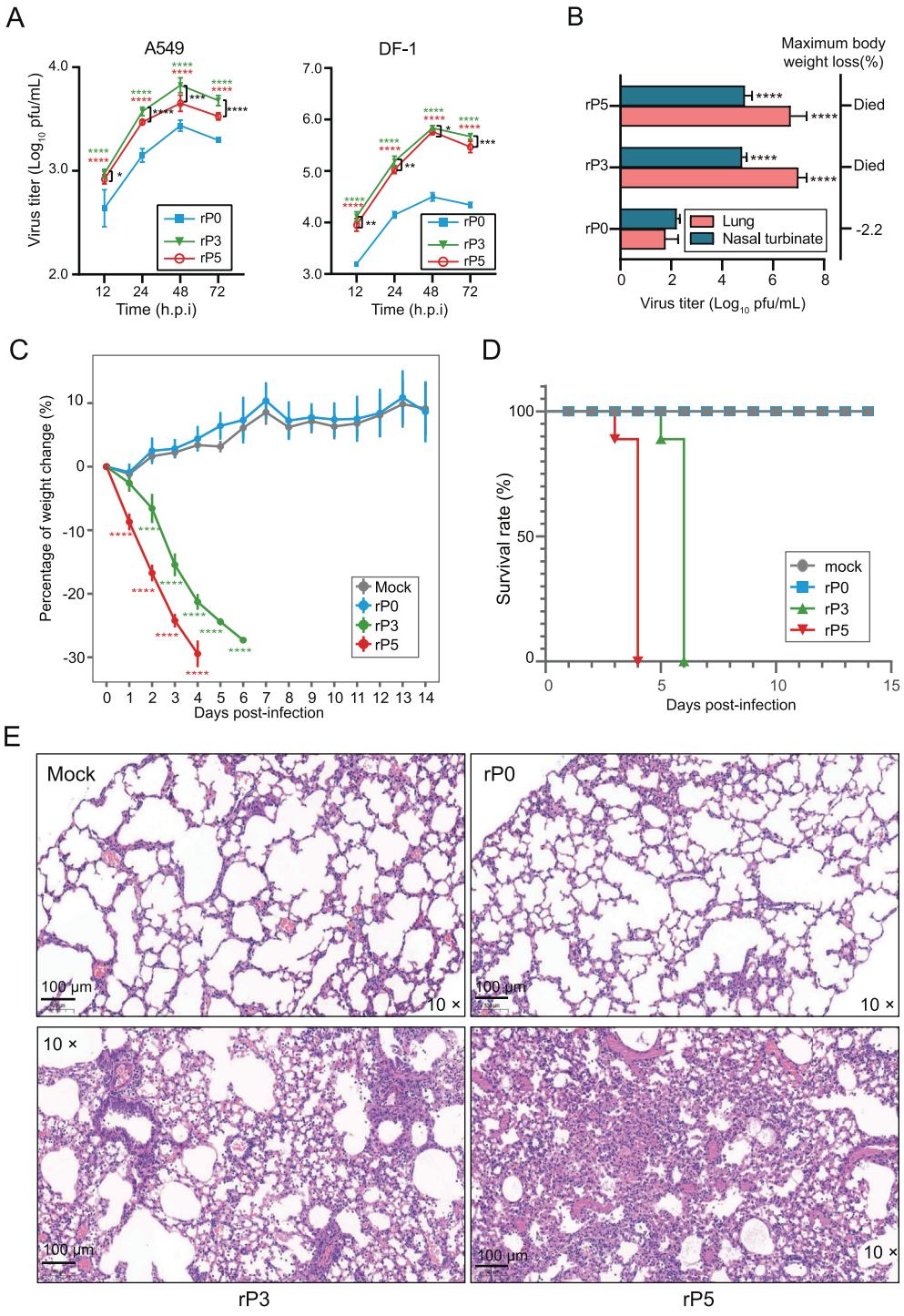

Fig. 2. Replication and pathogenicity of rP0, rP3, and rP5 viruses *in vitro* and *in vivo*. **A** Growth kinetics of 3W3 rP0, rP3, and rP5 viruses in A549 and DF-1 cell lines. Cells were infected with the indicated viruses at MOI of 0.01, and the supernatants of indicated time were collected for viral titer detection by plague assay. The experiment was performed three times. **B** Viral titers of 3W3 rP0, rP3, and rP5 viruses in mouse lung and nasal turbinate at 3 d.p.i. Three 6-week-old female BALB/c mice were inoculated with either 50 μL of the indicated viruses (10^5 PFU) or 50 μL 0.1% BSA-PBS (mock group). Body weight changes (**C**) and survival rates (**D**) were observed over 14 days (n = 5/group). Mice lost ≥25% of their body weight were considered as dead and sacrificed. Data are presented as the means ± standard deviations. Two-tailed unpaired *t*-test, $^*P < 0.05$, $^{**}P < 0.01$, $^{***}P < 0.001$, $^{****}P < 0.0001$. **E** Lung histopathology of mice infected with 3W3 rP0, rP3, and rP5 viruses. The images were gained at ×10 magnification and bars of the enlarged images represented 100 μm.

rP0-infected mice, mice infected with the rP0-P5PA virus showed no clinical signs or weight loss. However, histopathological examination of infected mice lungs at 3 d.p.i. indicated that both rP0-P3HA and rP0-P5PA viruses caused lung injury including thickening of alveolar walls, hemorrhage, and inflammatory cell infiltration (Supplementary Fig. S2). These results suggest that the HA-L226Q, T511I, and A528V substitutions were responsible for the enhanced pathogenicity of the 3W3-mouse-adapted virus.

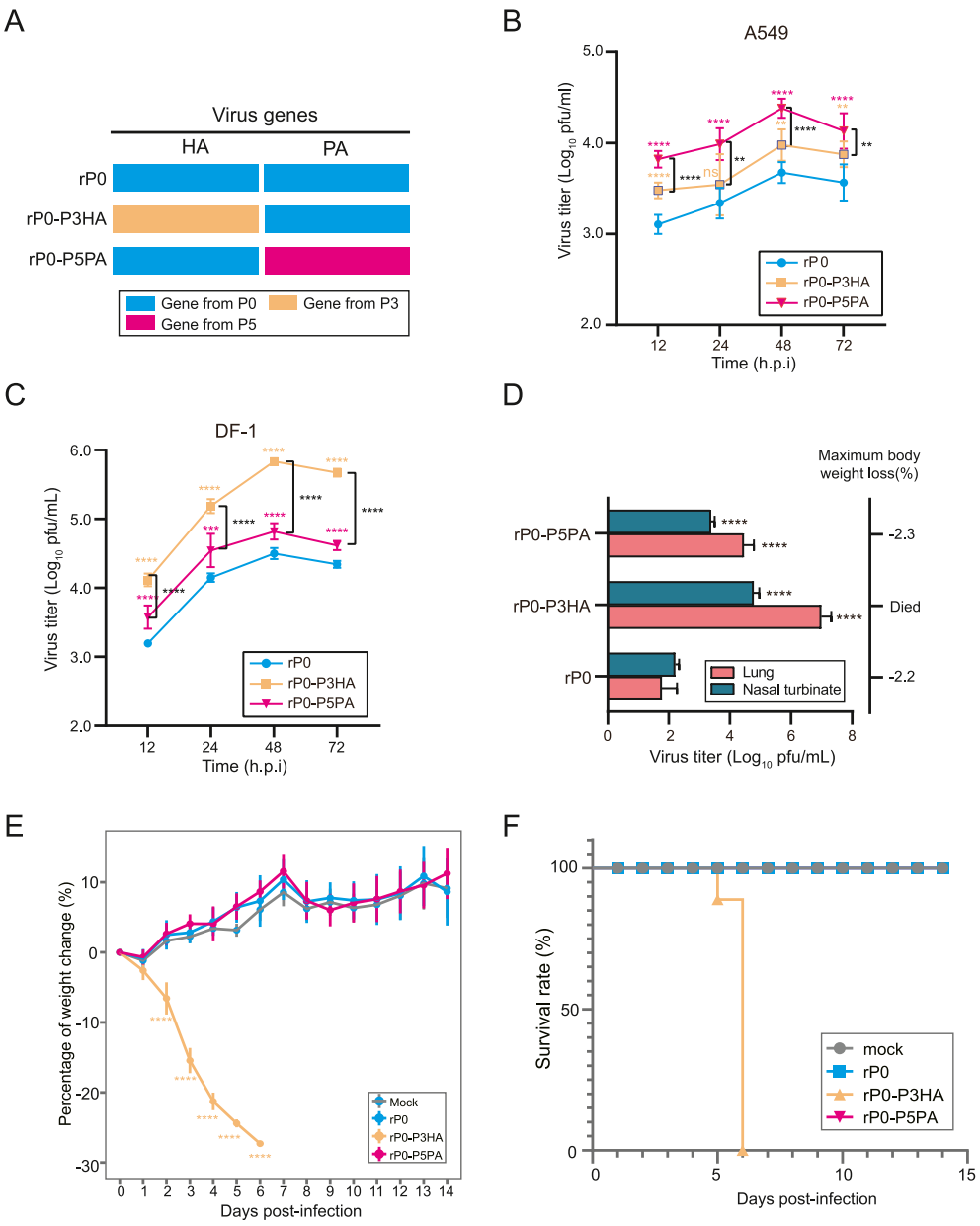

Fig. 3. Replication and pathogenicity of rP0-P3HA and rP0-P5PA recombinant viruses *in vitro* and *in vivo*. **A** Workflow of segment replacement in recombinant viruses. The rP0-P3HA and rP0-P5PA viruses were generated by replacing the HA or PA segments of rP0 virus, respectively. (**B–C**) Growth kinetics of 3W3 rP0, rP0-P3HA, and rP0-P5PA viruses in A549 and DF-1 cell lines. Cells were infected with the indicated viruses at MOI of 0.01, and the supernatants of indicated time were collected for viral titer detection by plague assay. The experiment was performed three times. **D** Viral titers in mouse lung and nasal turbinates infected with 3W3 rP0, rP0-P3HA, and rP0-P5PA viruses at 3 d.p.i. (n = 3/group, 10^5 PFU/mouse). **E** Body weight changes and survival rates (**F**) were observed over 14 days (n = 5/group). Mice lost ≥25% of their body weight were considered as dead and sacrificed. Data are presented as the means ± standard deviations. Two-tailed unpaired *t*-test, $^*P < 0.05$, $^{**}P < 0.01$, $^{***}P < 0.001$, $^{****}P < 0.0001$.

3.4. HA-L226Q was the key factor of enhanced pathogenicity in vivo and the receptor-binding preference

To identify the exact amino acid sites of HA responsible for enhanced replication and pathogenicity, we generated recombinant viruses bearing HA-L226Q, HA-T511I, or HA-A528V substitutions (namely rP0-HA-L226Q, rP0-HA-T511I, and rP0-HA-A528V, respectively). The growth kinetics of rP0-HA-L226Q, rP0-HA-T511I, and rP0-HA-A528V viruses in A549 cells were significantly increased at 24 h.p.i., 48 h.p.i., and 72 h.p.i. compared with those of the rP0 virus, among which the rP0-HA-L226Q virus produced the highest viral titer. In DF-1 cells, we observed increased replication of rP0-HA-L226Q, rP0-HA-T511I, and rP0-HA-A528V compared with the rP0 virus at 12 h.p.i. and 24 h.p.i., and the rP0-HA-L226Q virus also replicated to the highest viral titer at 12 h.p.i. and 24 h.p.i. (Fig. 4A). However, the replication rates of rP0-HA-T511I and rP0-HA-A528V viruses were significantly reduced compared with those of the rP0 virus at 72 h.p.i. in DF-1 cells. Furthermore, it was observed that most DF-1 cells infected with the rP0-HA-L226Q virus died after 24 h.p.i. This was contributed to a significant reduction in viral titers at 48 and 72 h.p.i., as depicted in Fig. 4A.

To test the effect of the three HA mutations on the pathogenicity, BALB/c mice were intranasally inoculated with 10^5 PFU of rP0, rP0-HA-L226Q, rP0-HA-T511I, or rP0-HA-A528V virus. We detected virus titers in the lungs and nasal turbinates of inoculated mice at 3 d.p.i.

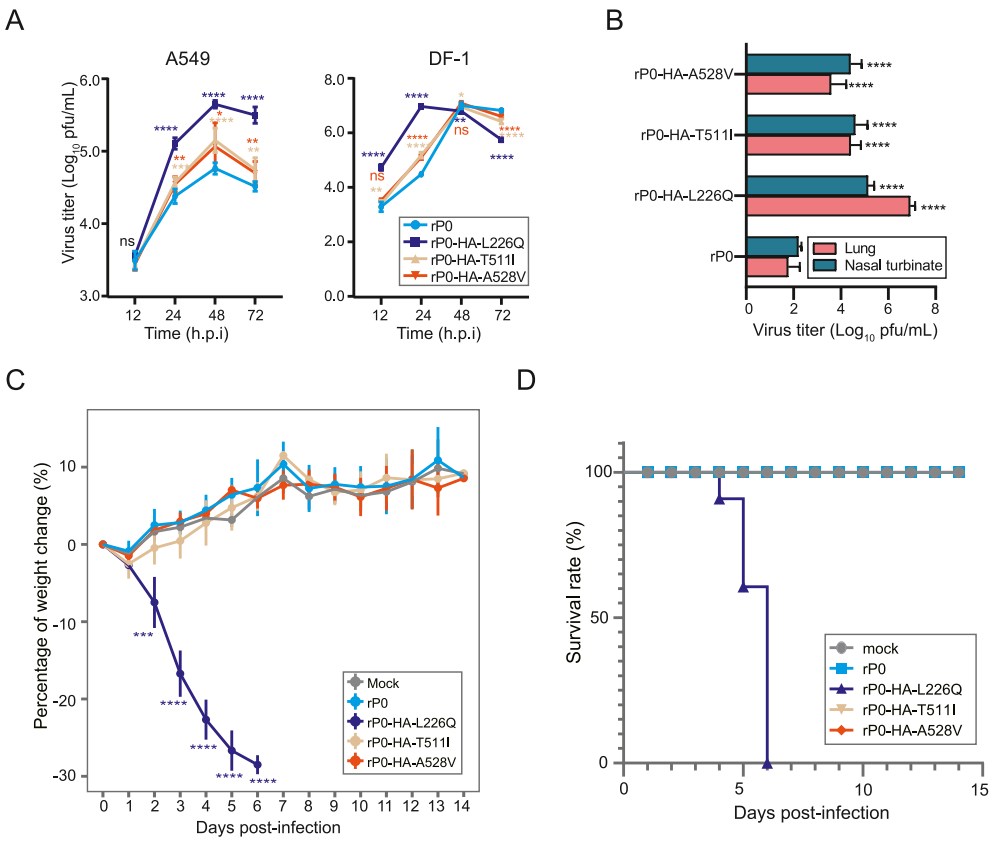

Fig. 4. Replication and pathogenicity of HA single mutation recombinant viruses *in vitro* and *in vivo*. **A** Growth kinetics of 3W3 rP0, rP0-HA-L226Q, rP0-HA-T511I, and rP0-HA-A528V viruses in A549 and DF-1 cell lines. Cells were infected with the indicated viruses at MOI of 0.01, and the supernatants of indicated time were collected for viral titer detection by plague assay. The experiment was performed three times. Most of the DF-1 cells infected with rP0-HA-L226Q virus died after 24 h.p.i. (**B–D**) Six-week-old female BALB/c mice intranasally with either 50 μL of the indicated viruses (10^5 PFU) or 50 μL of 0.1% BSA-PBS (mock group). Viral titers in mouse lungs and nasal turbinates (**B**) were detected at 3 d.p.i (n = 3/group). Body weight changes (**C**) and survival rates (**D**) (n = 5/group) were observed over 14 days. Mice lost ≥25% of their body weight were considered as dead and sacrificed. Data are shown as the means ± standard deviations, Two-tailed unpaired *t*-test, $*P < 0.05$, $**P < 0.01$, $***P < 0.001$, $****P < 0.0001$.

and observed that these were significantly higher in mice infected with rP0-HA-L226Q, rP0-HA-T511I, or rP0-HA-A528V viruses than those infected with rP0 ($P < 0.0001$, two-tailed unpaired *t*-test), with rP0-HA-L226Q showing the highest viral titers (Fig. 4B). Significant weight loss and death rates were observed only in rP0-HA-L226Q-inoculated mice (Fig. 4C and D), whereas no weight loss or death was observed in the rP0-HA-T511I or rP0-HA-A528V groups, suggesting that HA-L226Q was the key factor enhancing pathogenicity in mice.

Lung histopathology of infected mice showed that the three HA single-point mutation viruses caused varying degrees of lung tissue damage, among which the pathological changes caused by the rP0-HA-L226Q virus were more severe than those caused by rP0-HA-T511I and rP0-HA-A528V viruses. Lungs infected with the rP0-HA-L226Q virus revealed a local alveolar blockage, inflammatory cell infiltration, and thickening of alveolar walls (Supplementary Fig. S2). Mouse lungs inoculated with rP0-HA-T511I and rP0-HA-A528V viruses showed similar pathological changes, both of which formed local blockages; however, alveolar wall thickening was more severe in rP0-HA-T511I-infected mice (Supplementary Fig. S2). These results indicated that HA-L226Q, -T511I, and -A528V could enhance replication capability and pathogenicity, and the HA-L226Q mutation was the key factor.

In addition, to investigate whether HA mutations have an effect on viral receptor-binding properties, we examined the receptor-binding specificity of HA-mutated recombinant viruses using the solid-phase direct binding assay (Bi et al., 2015; Yao et al., 2022). As shown in Supplementary Fig. S3, rP0, rP0-HA-T511I, and rP0-HA-A528V viruses possessed dual-receptor binding property, while the rP0-HA-L226Q and rP3 viruses only bound to α-2,3-linked glycans (Supplementary Fig. S3), indicating HA-L226Q was the crucial mutation that altered the viral receptor-binding properties.

3.5. PA-T97I, PA-I545V, and PA-S594G contributed to enhancing viral replication in vitro and in vivo

To assess the roles of substitutions in the *PA* gene in replication and pathogenicity, we rescued recombinant 3W3 viruses possessing PA-T97I, PA-I545V, or PA-S594G, namely rP0-PA-T97I, rP0-PA-I545V, and rP0-PA-S594G, respectively. Multiple replication cycle growth curves in A549 cells showed that rP0-PA-T97I, rP0-PA-I545V, and rP0-PA-S594G viruses produced significantly higher viral titers than rP0 virus at 24 h.p.i., 48 h.p.i., and 72 h.p.i. ($P < 0.0001$), among which the rP0-PA-T97I virus produced the highest viral titer (Fig. 5A). However, the growth kinetics in DF-1 cells indicated that PA-I545V and PA-S594G mutations could promote viral replication at 24 h.p.i., whereas PA-T97I substitution inhibited replication throughout the viral replication cycle (Fig. 5B). These findings suggest that the three substitutions in the *PA* gene can enhance viral replication in mammalian cells.

We assessed the role of PA mutations in replication and pathogenicity in BALB/c mice. Although we did not observe any significant changes in weight loss or death rates (Fig. 5C), significantly higher viral titers were

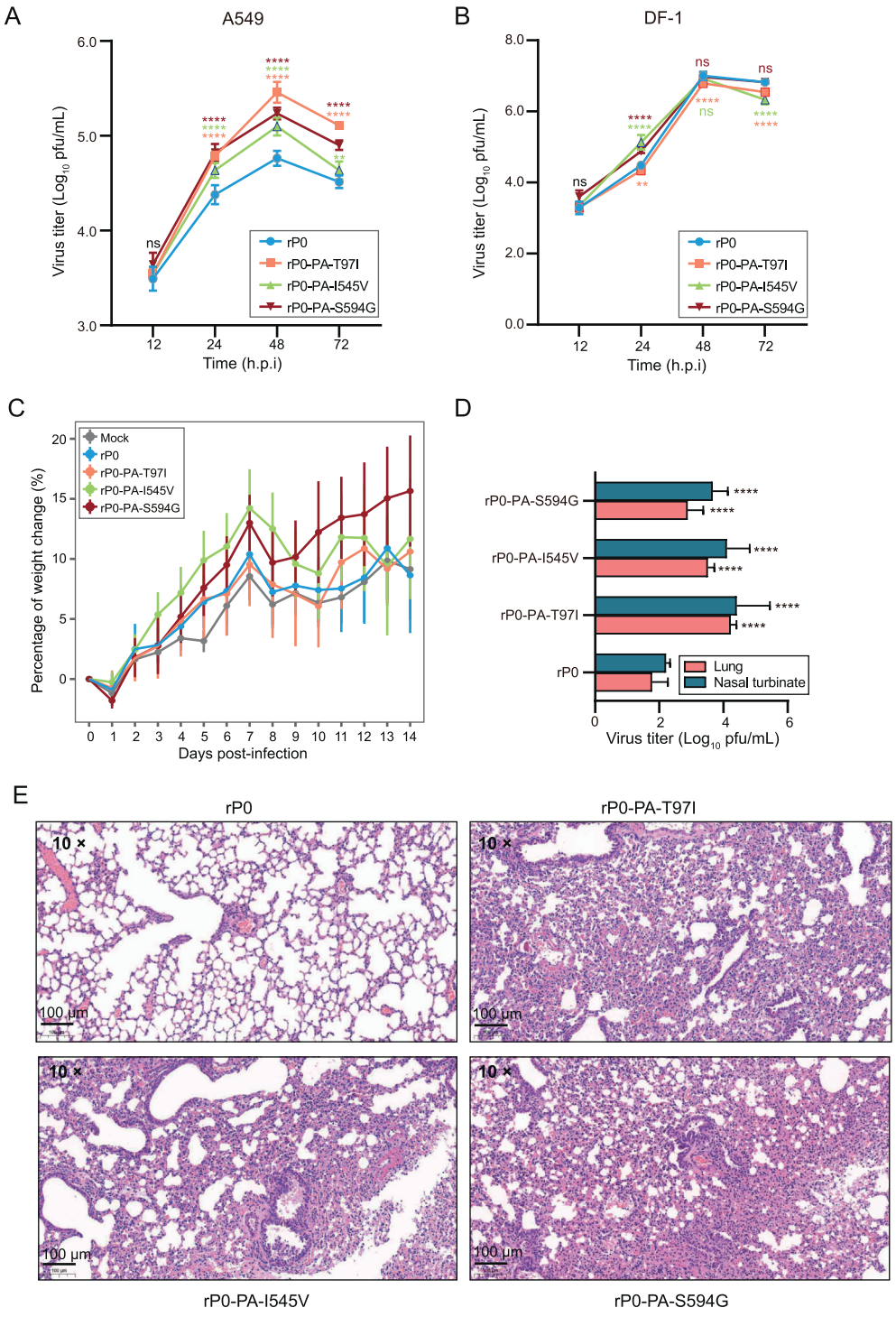

Fig. 5. Effect of PA substitutions in replication and pathogenicity. Growth kinetics of 3W3 rP0, rP0-PA-T97I, rP0-PA-I545V, and rP0-PA-S594G viruses in A549 (**A**) and DF-1 (**B**) cell lines. Cells were infected with the indicated viruses at MOI of 0.01, and the supernatants of indicated time were collected for viral titer detection by plague assay. The experiment was performed three times. **C** Body weight changes are presented as the means ± standard deviations (n = 5/group, 14 days period). **D** Virus titers of mouse lung and nasal turbinates infected with 3W3 rP0, rP0-PA-T97I, rP0-PA-I545V, and rP0-PA-S594G viruses at 3 d.p.i. (n = 3/group, 10^5 PFU/mouse). Two-tailed unpaired *t*-test, $^*P < 0.05$, $^{**}P < 0.01$, $^{***}P < 0.001$, $^{****}P < 0.0001$. **E** Lung histopathology of mice infected with rP0-PA-T97I, rP0-PA-I545V, and rP0-PA-S594G viruses at 3 d.p.i. The images were gained at ×10 magnification and bars of the enlarged images represented 100 μm.

observed in the lungs and nasal turbinates of mice infected with rP0-PA-T97I, rP0-PA-I545V, or rP0-PA-S594G viruses at 3 d.p.i. than those with rP0 virus infection ($P < 0.0001$, Fig. 5D). Lung histopathology of mice infected with rP0-PA-T97I, rP0-PA-I545V, and rP0-PA-S594G showed alveolar wall thickening and local blockage, inflammatory cell infiltration, and peribronchial inflammation (Fig. 5E). These results suggest that PA-T97I, -I545V, and -S594G contribute to enhancing viral replication *in vitro* and *in vivo*.

3.6. PA-T97I enhanced viral polymerase activity by accelerating viral polymerase complex assembly

To explore the effect of the three PA mutations on the transcriptional activity of RNP complexes, a luciferase mini-genome assay was performed in 293T and DF-1 cells. We observed significantly increased polymerase activity in mammalian cells of the PA-T97I, PA-T97I+I545V, PA-T97I+S594G, and PA-T97I+I545V+S594G groups than that in the PA group ($P < 0.0001$, Fig. 6A), and the polymerase activity of the PA-I545V, PA-S594G, and PA-I545V+S594G groups showed no significant difference compared with that in the PA group (Fig. 6A). These results suggest that PA-T97I enhances the transcriptional activity of the RNP complexes.

The polymerase activity in the PA-T97I+I545V and PA-T97I+I545V+S594G groups was significantly increased compared with that in the PA-T97I group ($P < 0.0001$), whereas that in the PA-T97I+S594G group was similar to that in the PA-T97I group (Fig. 6A). These results suggest that Val-545 in PA acted synergistically with Ile-97 in enhancing polymerase activity. However, a significant decrease in viral polymerase activity was observed in the PA-T97I- ($P < 0.01$) and PA-T97I+S594G-transfected DF-1 cells ($P < 0.05$) compared with that in the PA group (Fig. 6B), which is in contrast to the results for 293T cells.

Based on the role of PA-T97I in increasing polymerase activity, we tested the impact of PA-T97I on polymerase assembly. We observed that the amount of PB2 and PB1 immunoprecipitated by PA-T97I and PA-T97I+I545V+S594G increased compared to that with PA-WT, implying

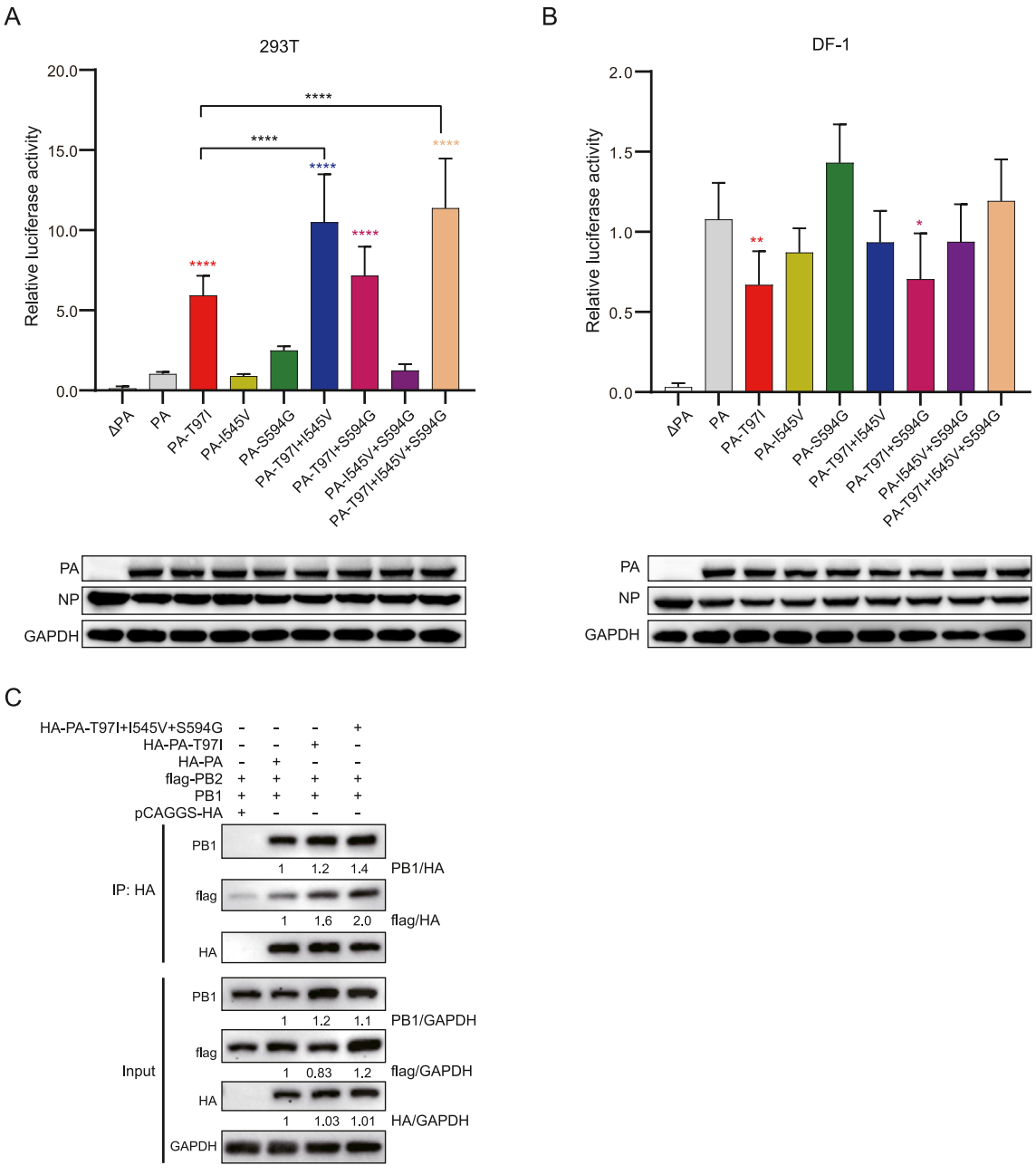

Fig. 6. Effect of PA mutations in viral polymerase activity and assembly. Polymerase activity of RNP complexes with different PA mutation combinations in 293T (**A**) and DF-1 (**B**) cells. Data are shown as the means ± standard deviations. One-way ANOVA, $^{*}P < 0.05$, $^{**}P < 0.01$, $^{***}P < 0.001$, $^{****}P < 0.0001$. **C** Effect of PA-T97I on polymerase assembly. 293T cells were transfected with 0.75 μg HA-PA, HA-PA-T97I, or HA-PA-T97I+I545V+S594G, 0.75 μg flag-PB2, and 0.75 μg PB1; after 24 h transfection, cells were lysed and immunoprecipitated with anti-HA magnetic beads for Western blot assay. Each experiment was performed three times.

that PA-T97I could increase the assembly of the viral polymerase (Fig. 6C). These findings indicate that PA-T97I enhances viral polymerase activity by accelerating the polymerase complex assembly in mammalian cells.

3.7. PA-T97I and/or PA-I545V have an antagonistic effect with P3HA on viral replication

As indicated above, the viral replication efficiency of rP3 (three HA mutations) was higher than that of the rP5 virus (three HA and three PA mutations) in A549 cells. However, the replication efficiency of the rP0-P5PA virus (three PA mutations) was higher than that of the rP0-P3HA virus (rP3 virus, three HA mutations) in A549 cells. This prompted us to consider whether the mutations of the HA and PA proteins act antagonistically in viral replication. To determine the exact site of functional antagonism, we constructed 64 recombinant viruses with all the possible permutations and combinations of the three HA and three PA mutations on the background of the P0 virus. We assessed the growth kinetics of these recombinant viruses in A549 and DF-1 cells at an MOI of 0.01, respectively. To confirm whether measuring with plaque assay and quantitative PCR assay is similar, 11 key virus's stocks were tested by both assays. The data showed that the recombinant viruses have comparable plaque to genome ratios (Supplementary Fig. S4). After normalizing the viral titers of these recombinant viruses to that of rP0 (Supplementary Dataset S2), we visualized the results as heat maps. These maps revealed several mutation sites that appeared to contribute to the antagonism we had previously assumed. To explore the function of different sites or various combinations, diverse recombinant viruses were grouped and analyzed together in the followings.

Owing to the earlier appearance of the three HA mutations, we verified the PA mutation responsible for the antagonism. The replication efficiency of eight recombinant viruses, including P3HA (three HA mutations) combined with single-, double-, and triple-point PA mutations, were analyzed together. We observed that the replication efficiency of recombinant viruses combined with single- (except for PA-S594G) and double- or triple-point PA mutations was lower than that of the rP0-P3HA virus in A549 cells (Fig. 7A). Notably, the replication capacity of P3HA+P97, P3HA+P545, and P3HA+P97+545 recombinant viruses was even lower than that of the rP0 virus in A549 cells, suggesting that PA-T97I and/or PA-I545V act antagonistically with three HA mutations in viral replication (Fig. 7A). In DF-1 cells, similar results were revealed as the replication efficiency of P3HA+P97, P3HA+P545, P3HA+P97+545, P3HA+P545+594, and rP5 viruses was lower than the rP0-P3HA virus (Fig. 7A).

3.8. Double- and triple-point mutations of PA are antagonistic with HA-226Q

To determine the exact HA mutation site responsible for the functional antagonism of PA mutations, we analyzed 24 recombinant viruses containing single-point mutations of HA (HA-L226Q, T511I, A528V) combined with single-, double-, and triple-point PA mutations. We observed that the HA-L226Q single mutation significantly promoted viral replication in A549 cells (Fig. 4A). When combined with PA-T97I single-point mutation, the viral replication capacity of the recombinant viruses (H226+P97) was equivalent to that of the HA-L226Q single-point mutation virus (H226). However, when the HA-L226Q mutation was combined with randomized two of the three PA mutations, the rescued viruses had lower replication efficiency compared with that of the H226 virus. With the HA-L226Q mutation combined with all three PA mutations (P5PA+H226), the rescued virus had a lower replication efficiency than that of the H226 virus, even lower than that of the rP0 virus (Fig. 7B). These results implied that the double- and triple-point mutations of PA had functional antagonism with HA-226Q in viral replication, which was consistent with the results in the avian DF-1 cell line (only at 12 h.p.i. and 24 h.p.i.) (Fig. 7B). No obvious antagonism was observed when HA-T511I was combined with PA (only with triple-point PA mutation at 48 h.p.i. and 72 h.p.i.) (Fig. 7C). However, a synergistic effect was observed when HA-T511I was combined with the single-point PA mutations PA-I545V and PA-S594G, respectively, significantly increasing the viral titers of rP0-HA-T511I+PA-I545V (H511+P545) or rP0-HA-T511I+PA-S594G (H511+P594) in A549 cells than those of rP0-HA-T511I (H511) and rP0-PA-I545V (P545), or rP0-HA-T511I (H511) and rP0-PA-S594G (P594), respectively (Supplementary Fig. S5). For HA-A528V, antagonism was only observed when combined with PA-I545V (H528+P545) in A549 cells (Fig. 7D). A synergistic effect was observed in A549 cells when HA-A528V was combined with the single-point PA mutation S594G, leading to significantly higher viral titers for rP0-HA-A528V+PA-S594G (H528+P594) in A549 cells than those for rP0-HA-A528V (H528) or rP0-PA-S594G (P594) (Supplementary Fig. S5). These results demonstrate that double- and triple-point mutations in PA are antagonistic to HA-226Q.

3.9. Double-point mutations of HA are antagonistic with single-, double-, and triple-point mutations of PA

After testing the single-point mutation of HA combined with PA, we tested the double-point mutations of HA with PA in 24 recombinant viruses carrying double-point HA mutations (HA-L226Q+T511I, L226Q+A528V, and T511I+A528V) combined with single-, double-, and triple-point PA mutations. In A549 cells, the recombinant viruses containing the HA double-point mutation HA-L226Q (HA-L226Q+T511I and HA-L226Q+A528V) combined with PA-T97I and/or PA-I545V had lower viral titers than those of rP0-HA-L226Q+T511I (H226+511, Fig. 7E) or rP0-HA-L226Q+A528V (H226+528, Fig. 7F). HA-T511I and HA-A528V showed synergistic effect on viral replication *in vitro*, leading to significantly higher viral titers for rP0-HA-T511I+A528V (H511+528) than those for rP0-HA-T511I (H511) or rP0-HA-A528V (H528, Supplementary Fig. S5) in A549 cells. The recombinant viruses carrying HA-T511I+A528V with any combination of the three PA mutations had lower viral titers than those carrying HA-T511I+A528V (Fig. 7G), suggesting that HA-T511I+A528V also contributed to the antagonism of PA mutations. In DF-1, all the three double-point HA mutations working antagonistically with any combination of the three PA mutations (Fig. 7E–G). These results indicate that the double-point HA mutation had antagonistic effect with single-, double-, and triple-point mutations of PA on viral replication.

3.10. PA-97I and PA-545V, as well as HA-528V and PA-545V, were functionally antagonistic to viral replication in mammalian cells

The three additional PA mutations reduced the effect of HA mutations on viral replication; therefore, we assessed whether this was attributed to the antagonistic effect of the PA mutations themselves and whether the remaining mutations played a role. We analyzed 25 recombinant viruses (21 viruses are shown in Fig. 7) consisting of double-point PA mutations (PA-T97I+I545V, T97I+S594G, and I545V+S594G) combined with the remaining PA mutation or single-, double-, and triple-point mutations of HA in a P0 background. We found that the replication capacity at 24 h.p.i. and 48 h.p.i. of the recombinant virus containing a combination of PA-T97I and PA-I545V (P97+545) was lower than that of rP0-PA-T97I (P97) or rP0-PA-I545V (P545) virus in A549 cells (Fig. 8A), suggesting that the two PA mutation sites were functionally antagonistic to viral replication. The growth kinetics of PA-T97I+I545V in combination with the remaining four mutations showed that the antagonistic effect of PA-T97I and PA-I545V could be compensated for when combined with PA-S594G (rP0-P5PA) in A549 cells (Fig. 8A). However, the antagonistic effect on viral replication in A549 cells was even higher when PA-T97I+I545V was combined with double- or triple-point HA mutations at 72 h.p.i. (Fig. 8A). In DF-1, there was no functional antagonism between PA-T97I and PA-I545V; however, the replication capacity of the recombinant viruses possessing PA-T97I+I545V and single-point HA mutations

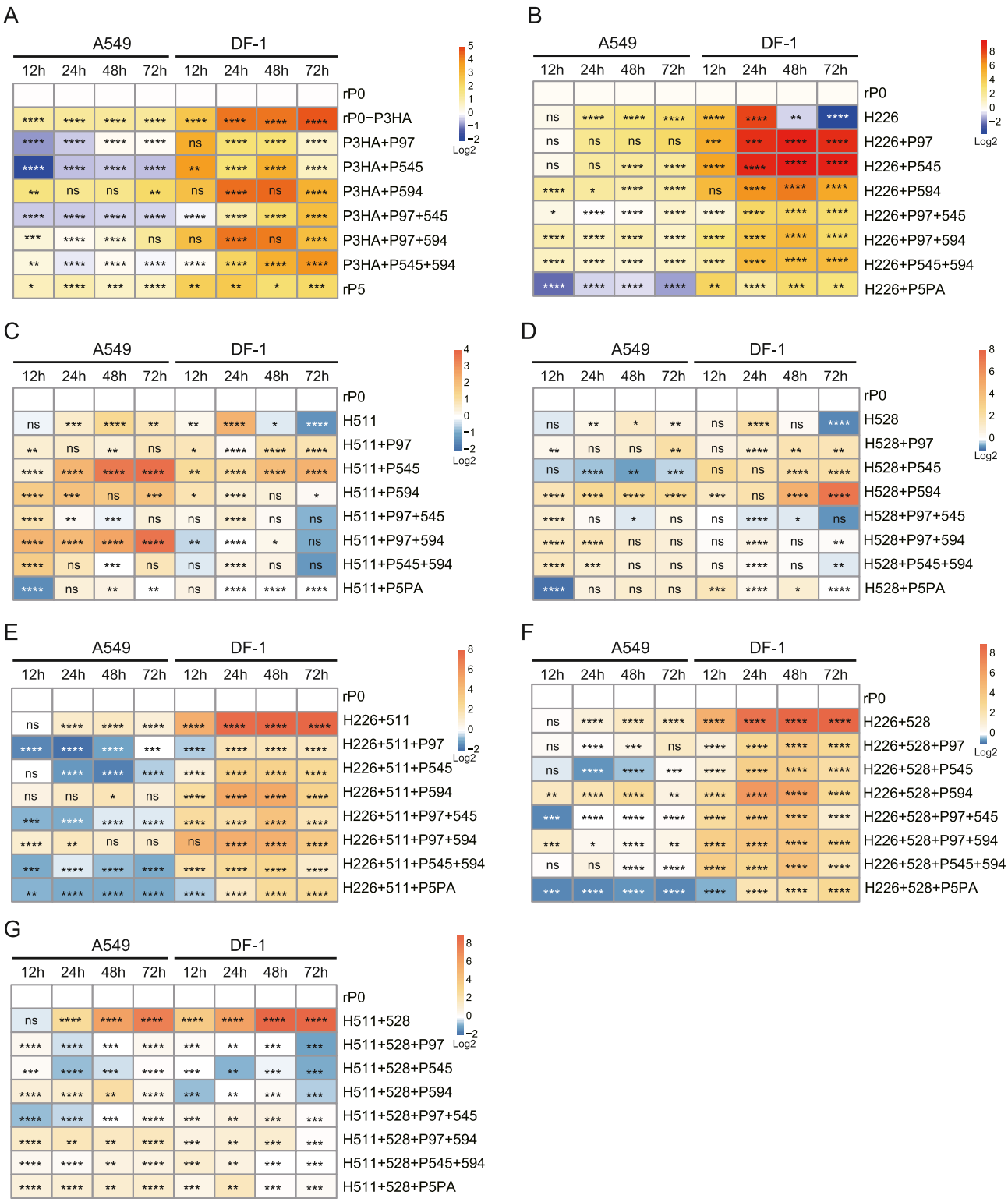

Fig. 7. Heat map of recombinant viruses with single-point HA mutation, double-point HA combination, and triple-point HA mutation respectively bombinated with the three mutations of PA. A549 and DF-1 cells were infected with recombinant viruses at MOI 0.01. The virus titers at various time points were normalized to those of rP0 and visualized as the Log_2 fold-change of that in rP0. Heat map of recombinant viruses carrying P3HA (three HA mutations) (**A**), HA-L226Q (**B**), HA-T511I (**C**), HA-A528V (**D**), HA-L226Q+T511I (**E**), HA-L226Q+A528V (**F**), and HA-T511I+A528V (**G**). In each case, growth kinetics were analyzed for eight recombinant viruses carrying the mutation/-s combined with single-point, double-point, and triple-point PA mutations in a P0 background and maintained in A549 and DF-1 cells. Each cell represents the fold change of virus titer (PFU/mL) at the given time point compared to that in the rP0 virus after Log_2 normalization. Each experiment was performed three times. The viral titers of each recombinant virus (except for rP0) in each panel were compared with those of the second virus, while viral titers of the second virus in each panel were compared with those of rP0. Two-tailed unpaired *t*-test, $*P < 0.05$, $**P < 0.01$, $***P < 0.001$, $****P < 0.0001$. P97, PA-T97I; P545, PA-I545V; P594, PA-S594G; H226, HA-L226Q; H511, HA-T511I; H528, HA-A528V.

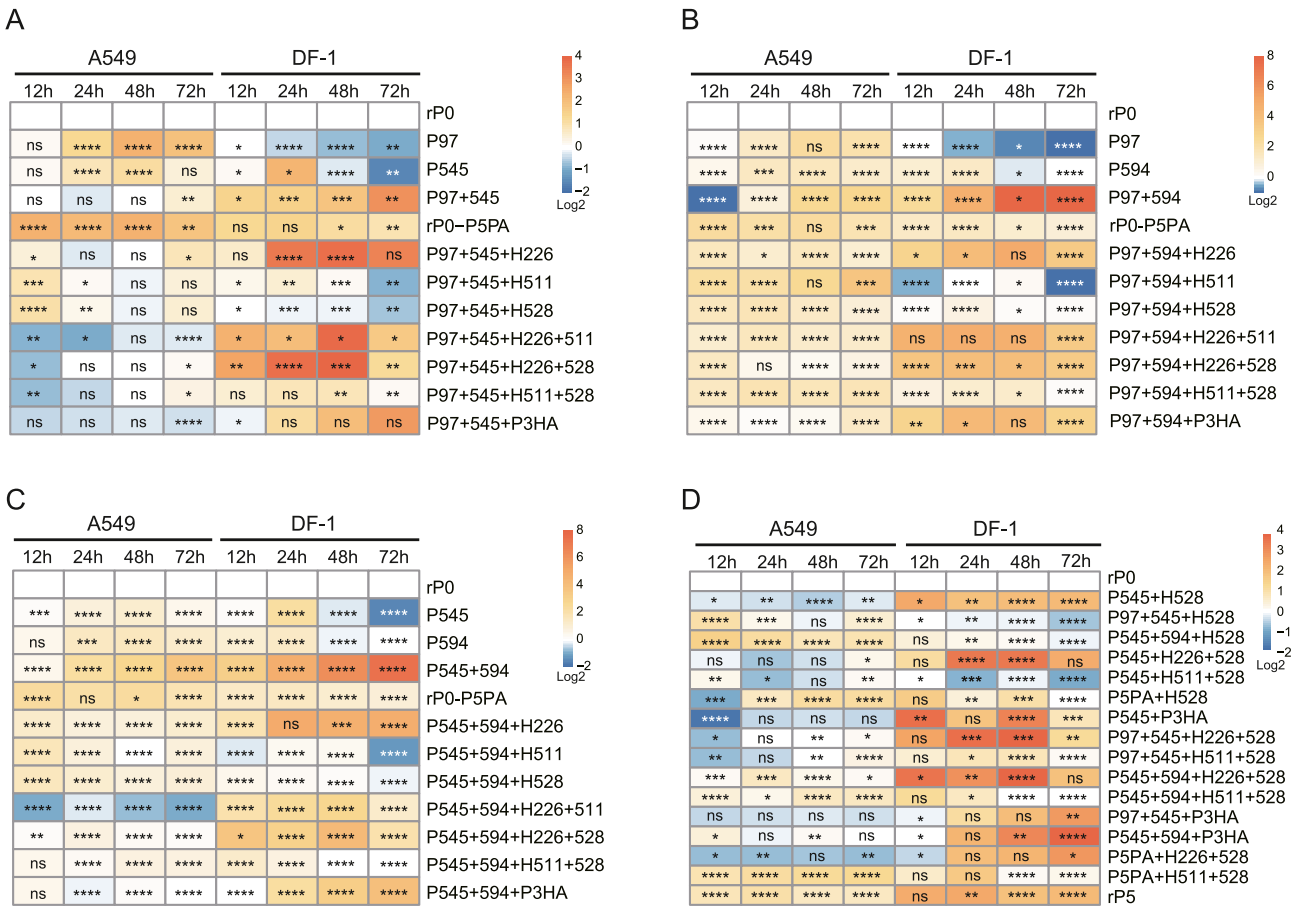

Fig. 8. Heat map of recombinant viruses harboring double-point PA mutations or PA-I545V+HA-A528V combined with remaining four mutations. A549 and DF-1 cells were infected with the recombinant virus at MOI = 0.01. Virus titers at various time points were normalized to those of rP0 and visualized as the Log_2 fold-change of that for rP0. Quantification of the growth curve of recombinant viruses carrying PA-T97I+I545V (**A**), PA-T97I+S594G (**B**), PA-I545V+S594G (**C**), and PA-I545V+HA-A528V (**D**). In each case, growth kinetics were analyzed for 11 (**A–C**) or 16 (**D**) recombinant viruses carrying the mutation/-s combined with the remaining four mutations in a P0 background and maintained in A549 and DF-1 cells. All viruses are included in Figs. 5 and 7. Only two of the viruses were newly analyzed for (**A**), one for (**B**), and one for (**C**). Each cell represents the fold change in virus titer (PFU/mL) at the indicated time point compared with that of the rP0 virus after Log_2 normalization. Each experiment was performed three times. The viral titers of each recombinant virus (except for rP0) in (**A–C**) were compared with those of fourth virus in each panel, while the viral titers of the fourth virus in each panel were compared with those of rP0. The viral titers of every recombinant virus (except for rP0) in panel **D** were compared with those of the second virus, while the viral titers of the second virus were compared with those of rP0. Two-tailed unpaired *t*-test, $*P < 0.05$, $**P < 0.01$, $***P < 0.001$, $****P < 0.0001$. P97, PA-T97I; P545, PA-I545V; P594, PA-S594G; H226, HA-L226Q; H511, HA-T511I; H528, HA-A528V.

HA-T511I (P97+545+H511) and HA-A528V (P97+545+H528) was lower than that of the rP0 virus at the late stage of infection (Fig. 8A). These results indicate that PA-97I and PA-545V were antagonistic to viral replication in mammalian cells and that the antagonism of PA-T97I and PA-I545V was enhanced by the double- and triple-point HA mutations.

PA-T97I and S594G had a synergistic effect on viral replication in DF-1 cells, and the replication efficiency of rP0-PA-T97I+S594G (P97+594) was significantly higher than that of rP0-PA-T97I and rP0-PA-S594G, respectively (Fig. 8B and Supplementary Fig. S5). No distinct antagonistic effect was observed in A549 or DF-1 cells for recombinant viruses possessing PA-T97I+S594G combined with the remaining four mutations, except for the combination with the single-point HA mutations A528V (P97+594+H528) and double- and triple-point mutations at 48 h.p.i. and 72 h.p.i. in A549 cells and the combination with the single-point HA mutations T511I (P97+594+H511) and A528V (P97+594+H528) in DF-1 cells (Fig. 8B). PA-I545V and S594G had synergistic effect on viral replication in both A549 and DF-1 cells: the replication efficiency of rP0-PA-I545V+S594G (P545+594) was significantly higher than that of rP0-PA-I545V (P545) and rP0-PA-S594G (P594) (Fig. 8C and Supplementary Fig. S5). However, antagonistic effect was observed in A549 cells for recombinant viruses possessing PA-I545V+S594G combined with single-, double-, or triple-point HA mutation recombinant viruses, especially when combined with HA-L226Q+T511I, suggesting that PA-I545V+S594G antagonizes viral replication with any combination of HA mutations in mammalian cells (Fig. 8C).

The replication efficiency of recombinant viruses possessing PA-I545V and HA-A528V was lower than that of the rP0 virus in A549 cells (Fig. 7D), which suggests that viral replication at these two sites was also antagonistic. To determine whether the other four mutations affected the functional antagonism of the PA-I545V and HA-A528V mutations, we analyzed the growth kinetics of recombinant viruses possessing PA-I545V+HA-A528V combined with single-, double-, triple-, and quadruple-point mutations of the remaining four mutations (corresponding to 16 recombinant viruses including P545+H528; Fig. 7, Fig. 8A, and Fig. 8C). We observed that the antagonistic effect of the combination of these two mutations could be compensated for when combined with other single-, double-, or triple-point mutations containing PA-S594G in A549 cells, except for P5PA+H226+528 (Fig. 8D). In DF-1 cells, PA-I545V+HA-A528V combined with PA-T97I (P97+545+H528) or HA-T511I (P545+H511+528) inhibited viral replication compared with that for the rP0 virus (Fig. 8D). These results indicate that PA-545V and HA-528V were antagonistic to viral replication in mammalian cells, which was alleviated by single-, double-, and triple-point mutations containing PA-594G.

4. Discussion

H9N2 AIVs pose a major public health risk owing to their distribution worldwide in live poultry markets and their broad host range (Li et al., 2017). Efficient replication and sustained transmission of AIVs in mammals require adaptations to survive in the host environment and overcome interspecies barriers. In this study, the 3W3 H9N2 virus was serially passaged in mouse lungs, and dynamic changes in its performance were monitored to explore the molecular basis of H9N2 mouse adaptation. Six mutations were identified in HA and PA proteins, four of which were newly described in IAVs. Using reverse genetics, we identified the genes and amino acid substitutions responsible for the enhanced pathogenicity and replication capacity of the 3W3 mouse-adapted virus. Furthermore, we observed that the effect of these six mutations on viral replication was not limited to linear superpositions; the antagonism between some mutations in HA and PA proteins may played crucial roles in the adaptation process.

Three mutations in the HA protein appeared rapidly during the second passage of the 3W3 virus (P2 virus). HA is the major glycoprotein on the surface of an IAV and is needed to bind to the sialic acid receptor (N-acetylneuraminic acid) on the surface of host cells, thereby mediating the membrane fusion of IAVs for internalization (Chauhan and Gordon, 2022). Given the roles of HA proteins, IAVs generally alter HA properties first to overcome interspecific barriers, which is consistent with our results. The P2 virus rapidly induced lethality in the mice and showed enhanced replication capacity and pathogenicity, which is detrimental to the co-evolution of the virus and host, and thus decreases the persistence of the virus in the host population. Therefore, the virus must use other proteins to balance the demand for replication and survival. PA, in our case, is a subunit with endonuclease activity in the IAV polymerase complex (Hara et al., 2006) and plays a vital role in the adaptation of IAVs (Sakabe et al., 2011; Zhu et al., 2012). The additional three mutations in PA (observed in P4–P5 viruses) were proven to alleviate the replication capabilities conferred by the three HA mutations in mammalian cells.

Mutations in HA were responsible for enhanced viral replication and pathogenicity and were predominantly determined by HA-L226Q. HA-L226Q was first found to change receptor specificity of H3 viruses (Rogers and Paulson, 1983), and then have also been reported in mouse-adapted viruses, such as H9N2 (Wang et al., 2012) and H7N9 (Zhao et al., 2016), but its effect on viral pathogenicity in mice was rarely involved. Recently, a study about engineering H9N2 vaccine strain verified that HA-L226Q could increase mouse pathogenicity (An et al., 2023), which is in accordance with our findings. Although in many previous studies, HA-226Q was considered as avian-specific (Connor et al., 1994; Lin et al., 2000; Matrosovich et al., 2000, 2001; Liu et al., 2023), we found a greater proportion of HA-226Q in mammalian H9N2 strains than that of avian H9N2 isolates, suggesting HA-L226Q may contribute to H9N2's adapting to mammals. In the lower respiratory tract, where the α-2,3 sialic acid receptor is predominant (Shinya et al., 2006), HA-L226Q functions as expected for the virus to adapt to the lung. HA-T511I and HA-A528V, which were newly described in IAVs, enhanced viral replication capacity in mammalian cells and mice and caused mild tissue damage in mouse lungs. HA-511 and -528 are both located in the HA2 domain; however, the mechanisms by which HA-T511I and A528V affect viral replication, pathogenicity, and cross-species transmission of H9N2 viruses in mammals remain unclear.

The three mutations of the *PA* gene were associated with enhanced viral replication ability in mice and mammalian cells. PA-T97I has been detected in mouse-adapted H5N1, H6N1, and H9N2 viruses and was shown to enhance viral polymerase activity in mammalian cells (Song et al., 2009; Cheng et al., 2014; Swieton et al., 2018), which is consistent with our findings. Additionally, we observed that Ile-97 in PA enhances viral polymerase activity by promoting the assembly of the polymerase complex. The other PA mutations, PA-I545V and PA-S594G, were also newly described in IAVs. In addition, the ratio of PA-545V in mammalian H9N2 strains was higher than that of avian H9N2 isolates, suggesting valine in PA-545 may be biased for H9N2 mammalian adaptation. The C-terminal domain of the PA protein is involved in host transcription factor hCLE interactions (Huarte et al., 2001; Ping et al., 2011) and PB1 binding (Ohtsu et al., 2002; He et al., 2008; Obayashi et al., 2008); PA-I545V and PA-S594G were both adjacent to the hCLE binding site. We inferred that PA-I545V and PA-S594G might affect the interaction between PA and hCLE to affect the modification of RNA synthesis (Nagata et al., 1989; Shimizu et al., 1994; Ping et al., 2011), though the exact mechanism by which the two PA mutations promote viral replication is unclear.

Our data showed that the three PA mutations impaired the contribution of the three HA mutations to replication efficiency *in vitro*. We found that multiple mutations in HA and PA proteins were functionally antagonistic to viral replication. According to a mini-genome replicon system, PA-T97I and PA-I545V synergistically enhanced viral polymerase activity in mammalian cells. However, PA-T97I and PA-I545V exerted antagonistic effect on live viral replication in the A549 cells. These seemingly contradictory results may be because the mini-genome replicon cannot completely replicate live virus replication. Meanwhile, the antagonistic effect of PA-T97I and PA-I545V on recombinant viral replication in A549 cells could be compensated for when combined with PA-S594G. Therefore, we hypothesized that the combined mutation of the amino acid sites in the *PA* gene is indispensable to maintaining a balance in viral replication. However, the detailed mechanism requires further investigation.

The study represents a pioneering effort to identify the antagonistic effect of mutations in HA and PA proteins on viral replication *in vitro*. Our findings suggest that this strategy may be involved in the mammalian adaptation of the H9N2 virus. Nonetheless, our study has certain limitations. Specifically, while we have demonstrated the antagonism of these mutation sites on viral replication at the cellular level, it remains unclear whether these sites have similar effect on viral replication *in vivo* and whether antagonism at these sites contributes to viral evasion of host immune surveillance. These gaps in knowledge present opportunities for further research in this area. Overall, our study underscores the molecular mechanism underlying the adaptation of avian H9N2 virus to mammalian hosts, highlighting the importance of balancing trade-offs during adaptation for viruses to persist in host populations. These findings may have crucial implications for understanding the molecular basis of viral pathogenesis and the development of effective antiviral treatments.

5. Conclusions

In summary, we investigated the genetic changes of a chicken-isolated H9N2 virus during mouse adaptation, and identified six mutations in HA and PA proteins that enhance replication efficiency and pathogenicity *in vitro* and *in vivo*. Furthermore, we observed the antagonistic effect of certain mutations in the HA and PA proteins on viral replication. Our study describes a genetic mechanism by which H9N2 adapts to mammalian hosts and highlights the importance of balancing trade-offs during adaptation for viruses to persist in the mammalian host population.

Data availability

All the data of this study are included in this manuscript. The sequences of the 3W3 virus can be found in the GISAID database (https://gisaid.org/) (Accession number: P0: EPI2397748–EPI2397755, P1: EPI2397700–EPI2397707, P2: EPI2397716–EPI2397723, P3: EPI2397724–EPI2397731, P4: EPI2397732–EPI2397739, P5: EPI2397740–EPI2397747). All data relevant to this study are available upon request from the corresponding author.

Ethics statement

All animal experiments were conducted in an Animal Biosafety Level 2 (ABSL-2) laboratory according to the Guide for the Care and Use of Laboratory Animals of the Ministry of Science and Technology of the People's Republic of China and were approved by the Animal Experimental Ethics Committee of the Wuhan Institute of Virology, Chinese Academy of Sciences (approval number WIVA04201901 and WIVA04202104).

Author contributions

Liping Ma: methodology, investigation, formal analysis, data curation, writing original draft. Huabin Zheng: methodology, investigation. Xianliang Ke: methodology, investigation. Rui Gui: methodology, investigation. Zhongzi Yao: methodology, investigation. Jiasong Xiong: methodology, investigation. Quanjiao Chen: supervision, funding acquisition.

Conflict of interest

The authors declare that they have no conflict of interest.

Acknowledgements

This work was supported by the National Key Research and Development Program of China (NKPs) (2022YFC2604101) and the National Science and Technology Major Project of China (2020ZX10001016-002). We are grateful for the technical support of the Institutional Center for Shared Technologies and Facilities of Wuhan Institute of Virology, CAS (Center for Instrumental Analysis and Metrology and Center for Animal Experiment).

Appendix A. Supplementary data

Supplementary data to this article can be found online at https://doi.org/10.1016/j.virs.2023.11.004.

References

Ali, M., Yaqub, T., Mukhtar, N., Imran, M., Ghafoor, A., Shahid, M.F., Naeem, S.M., Iqbal, M., Smith, G.J.D., Su, Y.C.F., 2019. Avian influenza A(H9N2) virus in poultry worker, Pakistan, 2015. Emerg. Infect. Dis. 25, 136–139.

Almayahi, Z.K., Al Kindi, H., Davies, C.T., Al-Rawahi, B., Al-Jardani, A., Al-Yaqoubi, F., Jang, Y., Jones, J., Barnes, J.R., Davis, W., Bo, S., Lynch, B., Wentworth, D.E., Al-Maskari, Z., Maani, A.A., Al-Abri, S., 2020. First report of human infection with avian influenza A(H9N2) virus in Oman: the need for a One Health approach. Int. J. Infect. Dis. 91, 169–173.

An, S.H., Hong, S.M., Song, J.H., Son, S.E., Lee, C.Y., Choi, K.S., Kwon, H.J., 2023. Engineering an optimal Y280-lineage H9N2 vaccine strain by tuning PB2 activity. Int. J. Mol. Sci. 24, 8840.

Bi, Y., Chen, Q., Wang, Q., Chen, J., Jin, T., Wong, G., Quan, C., Liu, J., Wu, J., Yin, R., Zhao, L., Li, M., Ding, Z., Zou, R., Xu, W., Li, H., Wang, H., Tian, K., Fu, G., Huang, Y., Shestopalov, A., Li, S., Xu, B., Yu, H., Luo, T., Lu, L., Xu, X., Luo, Y., Liu, Y., Shi, W., Liu, D., Gao, G.F., 2016. Genesis, evolution and prevalence of H5N6 avian influenza viruses in China. Cell Host Microbe 20, 810–821.

Bi, Y., Li, J., Li, S., Fu, G., Jin, T., Zhang, C., Yang, Y., Ma, Z., Tian, W., Li, J., Xiao, S., Li, L., Yin, R., Zhang, Y., Wang, L., Qin, Y., Yao, Z., Meng, F., Hu, D., Li, D., Wong, G., Liu, F., Lv, N., Wang, L., Fu, L., Yang, Y., Peng, Y., Ma, J., Sharshov, K., Shestopalov, A., Gulyaeva, M., Gao, G.F., Chen, J., Shi, Y., Liu, W.J., Chu, D., Huang, Y., Liu, Y., Liu, L., Liu, W., Chen, Q., Shi, W., 2020. Dominant subtype switch in avian influenza viruses during 2016-2019 in China. Nat. Commun. 11, 5909.

Bi, Y., Zhang, Z., Liu, W., Yin, Y., Hong, J., Li, X., Wang, H., Wong, G., Chen, J., Li, Y., Ru, W., Gao, R., Liu, D., Liu, Y., Zhou, B., Gao, G.F., Shi, W., Lei, F., 2015. Highly pathogenic avian influenza A(H5N1) virus struck migratory birds in China in 2015. Sci. Rep. 5, 12986.

Brown, E.G., Liu, H., Kit, L.C., Baird, S., Nesrallah, M., 2001. Pattern of mutation in the genome of influenza A virus on adaptation to increased virulence in the mouse lung: identification of functional themes. Proc. Natl. Acad. Sci. U. S. A. 98, 6883–6888.

Butt, K.M., Smith, G.J., Chen, H., Zhang, L.J., Leung, Y.H., Xu, K.M., Lim, W., Webster, R.G., Yuen, K.Y., Peiris, J.S., Guan, Y., 2005. Human infection with an avian H9N2 influenza A virus in Hong Kong in 2003. J. Clin. Microbiol. 43, 5760–5767.

Chang, P., Sadeyen, J.R., Bhat, S., Daines, R., Hussain, A., Yilmaz, H., Iqbal, M., 2023. Risk assessment of the newly emerged H7N9 avian influenza viruses. Emerg. Microbes Infect. 12, 2172965.

Chauhan, R.P., Gordon, M.L., 2022. An overview of influenza A virus genes, protein functions, and replication cycle highlighting important updates. Virus Genes 58, 255–269.

Chen, H., Yuan, H., Gao, R., Zhang, J., Wang, D., Xiong, Y., Fan, G., Yang, F., Li, X., Zhou, J., Zou, S., Yang, L., Chen, T., Dong, L., Bo, H., Zhao, X., Zhang, Y., Lan, Y., Bai, T., Dong, J., Li, Q., Wang, S., Zhang, Y., Li, H., Gong, T., Shi, Y., Ni, X., Li, J., Zhou, J., Fan, J., Wu, J., Zhou, X., Hu, M., Wan, J., Yang, W., Li, D., Wu, G., Feng, Z., Gao, G.F., Wang, Y., Jin, Q., Liu, M., Shu, Y., 2014. Clinical and epidemiological characteristics of a fatal case of avian influenza A H10N8 virus infection: a descriptive study. Lancet 383, 714–721.

Cheng, K., Yu, Z., Chai, H., Sun, W., Xin, Y., Zhang, Q., Huang, J., Zhang, K., Li, X., Yang, S., Wang, T., Zheng, X., Wang, H., Qin, C., Qian, J., Chen, H., Hua, Y., Gao, Y., Xia, X., 2014. PB2-E627K and PA-T97I substitutions enhance polymerase activity and confer a virulent phenotype to an H6N1 avian influenza virus in mice. Virology 468–470, 207–213.

Connor, R.J., Kawaoka, Y., Webster, R.G., Paulson, J.C., 1994. Receptor specificity in human, avian, and equine H2 and H3 influenza virus isolates. Virology 205, 17–23.

Dias, A., Bouvier, D., Crepin, T., Mccarthy, A.A., Hart, D.J., Baudin, F., Cusack, S., Ruigrok, R.W., 2009. The cap-snatching endonuclease of influenza virus polymerase resides in the PA subunit. Nature 458, 914–918.

Gao, X., Wang, N., Chen, Y., Gu, X., Huang, Y., Liu, Y., Jiang, F., Bai, J., Qi, L., Xin, S., Shi, Y., Wang, C., Liu, Y., 2021. Sequence characteristics and phylogenetic analysis of H9N2 subtype avian influenza A viruses detected from poultry and the environment in China, 2018. PeerJ 9, e12512.

Gomaa, M.R., El Rifay, A.S., Abu Zeid, D., Elabd, M.A., Elabd, E., Kandeil, A., Shama, N.M.A., Kamel, M.N., Marouf, M.A., Barakat, A., Refaey, S., Naguib, A., Mckenzie, P.P., Webby, R.J., Ali, M.A., Kayali, G., 2020. Incidence and seroprevalence of avian influenza in a cohort of backyard poultry growers, Egypt, August 2015-March 2019. Emerg. Infect. Dis. 26, 2129–2136.

Guan, Y., Shortridge, K.F., Krauss, S., Webster, R.G., 1999. Molecular characterization of H9N2 influenza viruses: were they the donors of the "internal" genes of H5N1 viruses in Hong Kong? Proc. Natl. Acad. Sci. U. S. A. 96, 9363–9367.

Guo, Q., Zou, L., Yu, J., Song, Y., Liang, L., Zhuang, X., Song, T., Wu, J., 2020. First human infection with avian influenza H9N2 - Guangdong Province, China, 2020. China CDC Wkly. 2, 545–548.

Hara, K., Schmidt, F.I., Crow, M., Brownlee, G.G., 2006. Amino acid residues in the N-terminal region of the PA subunit of influenza A virus RNA polymerase play a critical role in protein stability, endonuclease activity, cap binding, and virion RNA promoter binding. J. Virol. 80, 7789–7798.

He, X.J., Zhou, J., Bartlam, M., Zhang, R.G., Ma, J.Y., Lou, Z.Y., Li, X.M., Li, J.J., Joachimiak, A., Zeng, Z.H., Ge, R.W., Rao, Z.H., Liu, Y.F., 2008. Crystal structure of the polymerase PA(C)-PB1(N) complex from an avian influenza H5N1 virus. Nature 454, 1123–U1151.

Hemerka, J.N., Wang, D., Weng, Y.J., Lu, W.X., Kaushik, R.S., Jin, J., Harmon, A.F., Li, F., 2009. Detection and characterization of influenza A virus PA-PB2 interaction through a bimolecular fluorescence complementation assay. J. Virol. 83, 3944–3955.

Hoffmann, E., Neumann, G., Kawaoka, Y., Hobom, G., Webster, R.G., 2000. A DNA transfection system for generation of influenza A virus from eight plasmids. Proc. Natl. Acad. Sci. U. S. A. 97, 6108–6113.

Homme, P.J., Easterday, B.C., 1970. Avian influenza virus infections. I. Characteristics of influenza A-Turkey-Wisconsin-1966 virus. Avian Dis. 14, 66–74.

Hu, Z., Peng, F., Xiong, Z., Zhang, W., Li, T., Shi, Y., Xie, J., Jin, X., Huang, J., Xiao, H., Bi, D., Song, N., Li, Z., 2021. Genetic and molecular characterization of H9N2 avian influenza viruses isolated from live poultry markets in Hubei Province, Central China, 2013–2017. Virol. Sin. 36, 291–299.

Huang, Y., Li, X., Zhang, H., Chen, B., Jiang, Y., Yang, L., Zhu, W., Hu, S., Zhou, S., Tang, Y., Xiang, X., Li, F., Li, W., Gao, L., 2015. Human infection with an avian influenza A (H9N2) virus in the middle region of China. J. Med. Virol. 87, 1641–1648.

Huarte, M., Sanz-Ezquerro, J.J., Roncal, F., Ortin, J., Nieto, A., 2001. PA subunit from influenza virus polymerase complex interacts with a cellular protein with homology to a family of transcriptional activators. J. Virol. 75, 8597–8604.

Jallow, M.M., Fall, A., Barry, M.A., Diop, B., Sy, S., Goudiaby, D., Fall, M., Enouf, V., Niang, M.N., Dia, N., 2020. Genetic characterization of the first detected human case of low pathogenic avian influenza A/H9N2 in sub-Saharan Africa, Senegal. Emerg. Microbes Infect. 9, 1092–1095.

Kampmann, M.L., Fordyce, S.L., Avila-Arcos, M.C., Rasmussen, M., Willerslev, E., Nielsen, L.P., Gilbert, M.T., 2011. A simple method for the parallel deep sequencing of full influenza A genomes. J. Virol. Methods 178, 243–248.

Lam, T.T., Wang, J., Shen, Y., Zhou, B., Duan, L., Cheung, C.L., Ma, C., Lycett, S.J., Leung, C.Y., Chen, X., Li, L., Hong, W., Chai, Y., Zhou, L., Liang, H., Ou, Z., Liu, Y., Farooqui, A., Kelvin, D.J., Poon, L.L., Smith, D.K., Pybus, O.G., Leung, G.M., Shu, Y., Webster, R.G., Webby, R.J., Peiris, J.S., Rambaut, A., Zhu, H., Guan, Y., 2013. The genesis and source of the H7N9 influenza viruses causing human infections in China. Nature 502, 241–244.

Li, C., Wang, S.G., Bing, G.X., Carter, R.A., Wang, Z.J., Wang, J.L., Wang, C.X., Wang, L., Wu, G., Webster, R.G., Wang, Y.Q., Sun, H.L., Sun, Y.P., Liu, J.H., Pu, J., 2017. Genetic evolution of influenza H9N2 viruses isolated from various hosts in China from 1994 to 2013. Emerg. Microbes Infect. 6, e106.

Li, X., Tian, B., Jianfang, Z., Yongkun, C., Xiaodan, L., Wenfei, Z., Yan, L., Jing, T., Junfeng, G., Tao, C., Rongbao, G., Dayan, W., Shu, Y., 2017. A comprehensive retrospective study of the seroprevalence of H9N2 avian influenza viruses in occupationally exposed populations in China. PLoS One 12, e0178328.

Lin, Y.P., Shaw, M., Gregory, V., Cameron, K., Lim, W., Klimov, A., Subbarao, K., Guan, Y., Krauss, S., Shortridge, K., Webster, R., Cox, N., Hay, A., 2000. Avian-to-human

transmission of H9N2 subtype influenza A viruses: relationship between H9N2 and H5N1 human isolates. Proc. Natl. Acad. Sci. U. S. A. 97, 9654–9658.
Liu, D., Shi, W.F., Shi, Y., Wang, D.Y., Xiao, H.X., Li, W., Bi, Y.H., Wu, Y., Li, X.B., Yan, J.H., Liu, W.J., Zhao, G.P., Yang, W.Z., Wang, Y., Ma, J.C., Shu, Y.L., Lei, F.M., Gao, G.F., 2013. Origin and diversity of novel avian influenza A H7N9 viruses causing human infection: phylogenetic, structural, and coalescent analyses. Lancet 381, 1926–1932.
Liu, K., Guo, Y., Zheng, H., Ji, Z., Cai, M., Gao, R., Zhang, P., Liu, X., Xu, X., Wang, X., Liu, X., 2023. Enhanced pathogenicity and transmissibility of H9N2 avian influenza virus in mammals by hemagglutinin mutations combined with PB2-627K. Virol. Sin. 38, 47–55.
Liu, H.Q., Liu, X.F., Cheng, J., Peng, D.X., Jia, L.J., Huang, Y., 2003. Phylogenetic analysis of the hemagglutinin genes of twenty-six avian influenza viruses of subtype H9N2 isolated from chickens in China during 1996-2001. Avian Dis. 47, 116–127.
Ma, M.J., Zhao, T., Chen, S.H., Xia, X., Yang, X.X., Wang, G.L., Fang, L.Q., Ma, G.Y., Wu, M.N., Qian, Y.H., Dean, N.E., Yang, Y., Lu, B., Cao, W.C., 2018. Avian influenza A virus infection among workers at live poultry markets, China, 2013-2016. Emerg. Infect. Dis. 24, 1246–1256.
Matrosovich, M., Tuzikov, A., Bovin, N., Gambaryan, A., Klimov, A., Castrucci, M.R., Donatelli, I., Kawaoka, Y., 2000. Early alterations of the receptor-binding properties of H1, H2, and H3 avian influenza virus hemagglutinins after their introduction into mammals. J. Virol. 74, 8502–8512.
Matrosovich, M.N., Krauss, S., Webster, R.G., 2001. H9N2 influenza A viruses from poultry in Asia have human virus-like receptor specificity. Virology 281, 156–162.
Nagata, K., Takeuchi, K., Ishihama, A., 1989. In vitro synthesis of influenza viral RNA: biochemical complementation assay of factors required for influenza virus replication. J. Biochem. 106, 205–208.
Obayashi, E., Yoshida, H., Kawai, F., Shibayama, N., Kawaguchi, A., Nagata, K., Tame, J.R.H., Park, S.Y., 2008. The structural basis for an essential subunit interaction in influenza virus RNA polymerase. Nature 454, 1127–U1157.
Ohtsu, Y., Honda, Y., Sakata, Y., Kato, H., Toyoda, T., 2002. Fine mapping of the subunit binding sites of influenza virus RNA polymerase. Microbiol. Immunol. 46, 167–175.
Pan, Y., Cui, S., Sun, Y., Zhang, X., Ma, C., Shi, W., Peng, X., Lu, G., Zhang, D., Liu, Y., Wu, S., Yang, P., Wang, Q., 2018. Human infection with H9N2 avian influenza in northern China. Clin. Microbiol. Infect. 24, 321–323.
Peiris, M., Yuen, K.Y., Leung, C.W., Chan, K.H., Ip, P.L., Lai, R.W., Orr, W.K., Shortridge, K.F., 1999. Human infection with influenza H9N2. Lancet 354, 916–917.
Ping, J., Keleta, L., Forbes, N.E., Dankar, S., Stecho, W., Tyler, S., Zhou, Y., Babiuk, L., Weingartl, H., Halpin, R.A., Boyne, A., Bera, J., Hostetler, J., Fedorova, N.B., Proudfoot, K., Katzel, D.A., Stockwell, T.B., Ghedin, E., Spiro, D.J., Brown, E.G., 2011. Genomic and protein structural maps of adaptive evolution of human influenza A virus to increased virulence in the mouse. PLoS One 6, e21740.
Potdar, V., Hinge, D., Satav, A., Simoes, E.F., Yadav, P.D., Chadha, M.S., 2019. Laboratory-confirmed avian influenza A(H9N2) virus infection, India, 2019. Emerg. Infect. Dis. 25, 2328–2330.
Rogers, G.N., Paulson, J.C., 1983. Receptor determinants of human and animal influenza virus isolates: differences in receptor specificity of the H3 hemagglutinin based on species of origin. Virology 127, 361–373.
Sakabe, S., Ozawa, M., Takano, R., Iwastuki-Horimoto, K., Kawaoka, Y., 2011. Mutations in PA, NP, and HA of a pandemic (H1N1) 2009 influenza virus contribute to its adaptation to mice. Virus Res. 158, 124–129.
Shanmuganatham, K., Feeroz, M.M., Jones-Engel, L., Smith, G.J.D., Fourment, M., Walker, D., Mcclenaghan, L., Alam, S.M.R., Hasan, M.K., Seiler, P., Franks, J., Danner, A., Barman, S., Mckenzie, P., Krauss, S., Webby, R.J., Webster, R.G., 2013. Antigenic and molecular characterization of avian influenza A(H9N2) viruses, Bangladesh. Emerg. Infect. Dis. 19, 1393–1402.
Shen, Y.Y., Ke, C.W., Li, Q., Yuan, R.Y., Xiang, D., Jia, W.X., Yu, Y.D., Liu, L., Huang, C., Qi, W.B., Sikkema, R., Wu, J., Koopmans, M., Liao, M., 2016. Novel reassortant avian influenza A(H5N6) viruses in humans, Guangdong, China, 2015. Emerg. Infect. Dis. 22, 1507–1509.
Shimizu, K., Handa, H., Nakada, S., Nagata, K., 1994. Regulation of influenza virus RNA polymerase activity by cellular and viral factors. Nucleic Acids Res. 22, 5047–5053.
Shinya, K., Ebina, M., Yamada, S., Ono, M., Kasai, N., Kawaoka, Y., 2006. Avian flu: influenza virus receptors in the human airway. Nature 440, 435–436.
Song, M.S., Pascua, P.N., Lee, J.H., Baek, Y.H., Lee, O.J., Kim, C.J., Kim, H., Webby, R.J., Webster, R.G., Choi, Y.K., 2009. The polymerase acidic protein gene of influenza a virus contributes to pathogenicity in a mouse model. J. Virol. 83, 12325–12335.
Song, W.J., Qin, K., 2020. Human-infecting influenza A (H9N2) virus: a forgotten potential pandemic strain? Zoonoses Public Health 67, 203–212.
Swieton, E., Jozwiak, M., Minta, Z., Smietanka, K., 2018. Genetic characterization of H9N2 avian influenza viruses isolated from poultry in Poland during 2013/2014. Virus Genes 54, 67–76.
Um, S., Siegers, J.Y., Sar, B., Chin, S., Patel, S., Bunnary, S., Hak, M., Sor, S., Sokhen, O., Heng, S., Chau, D., Sothyra, T., Khalakdina, A., Mott, J.A., Olsen, S.J., Claes, F., Sovann, L., Karlsson, E.A., 2021. Human infection with avian influenza A(H9N2) virus, Cambodia, February 2021. Emerg. Infect. Dis. 27, 2742–2745.
Wang, J., Sun, Y., Xu, Q., Tan, Y., Pu, J., Yang, H., Brown, E.G., Liu, J., 2012. Mouse-adapted H9N2 influenza A virus PB2 protein M147L and E627K mutations are critical for high virulence. PLoS One 7, e40752.
Xu, K.M., Smith, G.J., Bahl, J., Duan, L., Tai, H., Vijaykrishna, D., Wang, J., Zhang, J.X., Li, K.S., Fan, X.H., Webster, R.G., Chen, H., Peiris, J.S., Guan, Y., 2007. The genesis and evolution of H9N2 influenza viruses in poultry from southern China, 2000 to 2005. J. Virol. 81, 10389–10401.
Yang, R., Sun, H., Gao, F., Luo, K., Huang, Z., Tong, Q., Song, H., Han, Q., Liu, J., Lan, Y., Qi, J., Li, H., Chen, S., Xu, M., Qiu, J., Zeng, G., Zhang, X., Huang, C., Pei, R., Zhan, Z., Ye, B., Guo, Y., Zhou, Y., Ye, W., Yao, D., Ren, M., Li, B., Yang, J., Wang, Y., Pu, J., Sun, Y., Shi, Y., Liu, W.J., Ou, X., Gao, G.F., Gao, L., Liu, J., 2022. Human infection of avian influenza A H3N8 virus and the viral origins: a descriptive study. Lancet Microbe 3, e824–e834.
Yao, Z., Zheng, H., Xiong, J., Ma, L., Gui, R., Zhu, G., Li, Y., Yang, G., Chen, G., Zhang, J., Chen, Q., 2022. Genetic and pathogenic characterization of avian influenza virus in migratory birds between 2015 and 2019 in Central China. Microbiol. Spectr. 10, e0165222.
Yuan, R., Liang, L., Wu, J., Kang, Y., Song, Y., Zou, L., Zhang, X., Ni, H., Ke, C., 2017. Human infection with an avian influenza A/H9N2 virus in Guangdong in 2016. J. Infect. 74, 422–425.
Zhao, Y., Yu, Z., Liu, L., Wang, T., Sun, W., Wang, C., Xia, Z., Gao, Y., Zhou, B., Qian, J., Xia, X., 2016. Adaptive amino acid substitutions enhance the virulence of a novel human H7N9 influenza virus in mice. Vet. Microbiol. 187, 8–14.
Zhu, W.F., Zhu, Y., Qin, K., Yu, Z.J., Gao, R.B., Yu, H.Y., Zhou, J.F., Shu, Y.L., 2012. Mutations in polymerase genes enhanced the virulence of 2009 pandemic H1N1 influenza virus in mice. PLoS One 7, e33383.